Article

Immunity

Adipose-tissue Treg cells restrain differentiation of stromal adipocyte precursors to promote insulin sensitivity and metabolic homeostasis

Graphical abstract

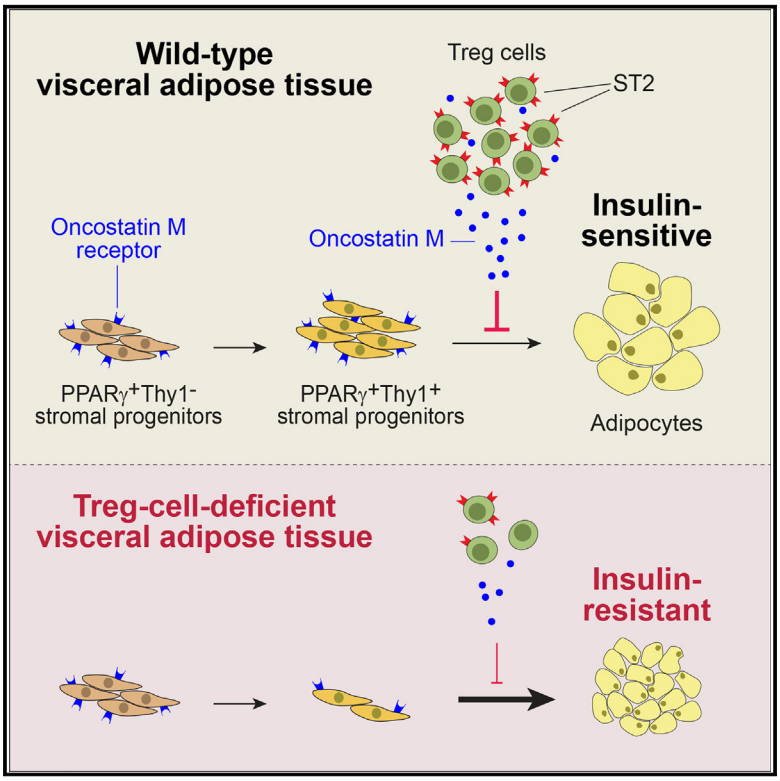

Highlights

- Visceral adipose tissue (VAT) hosts a distinct, polyfunctional Treg cell compartment
- Murine VAT-Treg cells rein in adipocyte differentiation from stromal precursors
- Oncostatin M is a major mediator of the anti-adipogenic effect of VAT-Treg cells
- Disruption of oncostatin-M signaling in mice results in profound insulin resistance

Authors

Gang Wang, Andrés R. Muñoz-Rojas, Raul German Spallanzani, Ruth A. Franklin, Christophe Benoist, Diane Mathis

Correspondence

dm@hms.harvard.edu

In brief

Regulatory T (Treg) cells in epididymal visceral adipose tissue (eVAT) regulate metabolic homeostasis. Wang et al. identify a distinct compartment of eVAT-Treg cells that rein in the differentiation of adipocytes from stromal progenitors via the molecular mediator oncostatin M, thereby promoting insulin sensitivity and metabolic health.

Wang et al., 2024, Immunity *57*, 1–15
June 11, 2024
https://doi.org/10.1016/j.immuni.2024.04.002

CellPress

Immunity

CellPress

Article

Adipose-tissue Treg cells restrain differentiation of stromal adipocyte precursors to promote insulin sensitivity and metabolic homeostasis

Gang Wang,[1] Andrés R. Muñoz-Rojas,[1] Raul German Spallanzani,[1,3] Ruth A. Franklin,[1,2] Christophe Benoist,[1] and Diane Mathis[1,4,*]

[1]Department of Immunology, Harvard Medical School, Boston, MA, USA
[2]Department of Stem Cell and Regenerative Biology, Harvard University, Cambridge, MA, USA
[3]Present address: KSQ Therapeutics, Lexington, MA, USA
[4]Lead contact
*Correspondence: dm@hms.harvard.edu
https://doi.org/10.1016/j.immuni.2024.04.002

SUMMARY

Regulatory T (Treg) cells in epididymal visceral adipose tissue (eVAT) of lean mice and humans regulate metabolic homeostasis. We found that constitutive or punctual depletion of eVAT-Treg cells reined in the differentiation of stromal adipocyte precursors. Co-culture of these precursors with conditional medium from eVAT-Treg cells limited their differentiation *in vitro*, suggesting a direct effect. Transcriptional comparison of adipocyte precursors, matured in the presence or absence of the eVAT-Treg-conditioned medium, identified the oncostatin-M (OSM) signaling pathway as a key distinction. Addition of OSM to *in vitro* cultures blocked the differentiation of adipocyte precursors, while co-addition of anti-OSM antibodies reversed the ability of the eVAT-Treg-conditioned medium to inhibit *in vitro* adipogenesis. Genetic depletion of OSM (specifically in Treg) cells or of the OSM receptor (specifically on stromal cells) strongly impaired insulin sensitivity and related metabolic indices. Thus, Treg-cell-mediated control of local progenitor cells maintains adipose tissue and metabolic homeostasis, a regulatory axis seemingly conserved in humans.

INTRODUCTION

White adipose tissue, in particular visceral adipose tissue (VAT), is responsible for systemic energy homeostasis in mammals. VAT dysfunction underlies a number of metabolic disorders, including obesity, insulin resistance, type 2 diabetes, and cardiovascular diseases.[1–3] Overnutrition is a common cause of such abnormalities, accompanied by adipocyte hypertrophy via lipogenesis, adipocyte hyperplasia through "adipogenesis," and/or fibrosis.[2,4] The ongoing epidemic of obesity, type 2 diabetes, and their comorbidities renders it imperative to understand the positive and negative processes and factors that regulate VAT homeostasis.

It has long been recognized that VAT depots host a diversity of cell types beyond adipocytes,[5] a notion recently reinforced by studies exploiting single-cell RNA sequencing (scRNA-seq) technology.[6,7] A major non-adipocyte component of VAT, in particular the epididymal VAT (eVAT) depot, is immunocytes—notably pro- and anti-inflammatory macrophages (MFs), $CD4^+$ and $CD8^+$ effector T (Teff) cells, $Foxp3^+CD4^+$ regulatory T (Treg) cells, and natural-killer (NK) T cells and various types of innate lymphoid cells (ILCs). Among the diverse immunocyte classes in eVAT, Treg cells are particularly important regulators of local and systemic inflammation and metabolism.[8,9]

The eVAT-Treg population is a unique constellation of $Foxp3^+CD4^+$ T cells, adapted to survive in their challenging microenvironment and to suitably function therein. Their transcriptome, T cell receptor (TCR) repertoire, and growth and survival factor dependencies differ from those of Treg cells in lymphoid and other non-lymphoid tissues. Analogous to adipocytes, eVAT-Treg cells depend critically on the transcription factor (TF) PPARγ for their accumulation and function.[10] Mice lacking PPARγ, specifically in $Foxp3^+CD4^+$ T cells, have a much-reduced eVAT-Treg population but have normal Treg compartments in lymphoid organs and are largely resistant to the insulin-sensitizing effects of PPARγ agonists such as thiazolidinedione drugs. Genetically or nutritionally induced obesity results in a loss of eVAT, but not other, Treg cells—in particular, the major eVAT-Treg subtype expressing ST2, the receptor for IL-33.[10,11] This loss has variously been attributed to the toxic effects of type I interferon (IFN),[11] type II IFN,[12,13] or tumor necrosis factor (TNF)α,[14] or to heightened expression of a soluble ST2 decoy molecule,[14] each associated with a reduction in *Pparg* expression.[11]

A second major non-adipocyte component of the eVAT depot is stromal cells. We recently identified five subtypes of eVAT mesenchymal stromal cells (VmSCs) via scRNA-seq analysis,[15] a profile consistent with that of other reports.[6] Two PPARγ-expressing

Please cite this article in press as: Wang et al., Adipose-tissue Treg cells restrain differentiation of stromal adipocyte precursors to promote insulin sensitivity and metabolic homeostasis, Immunity (2024), https://doi.org/10.1016/j.immuni.2024.04.002

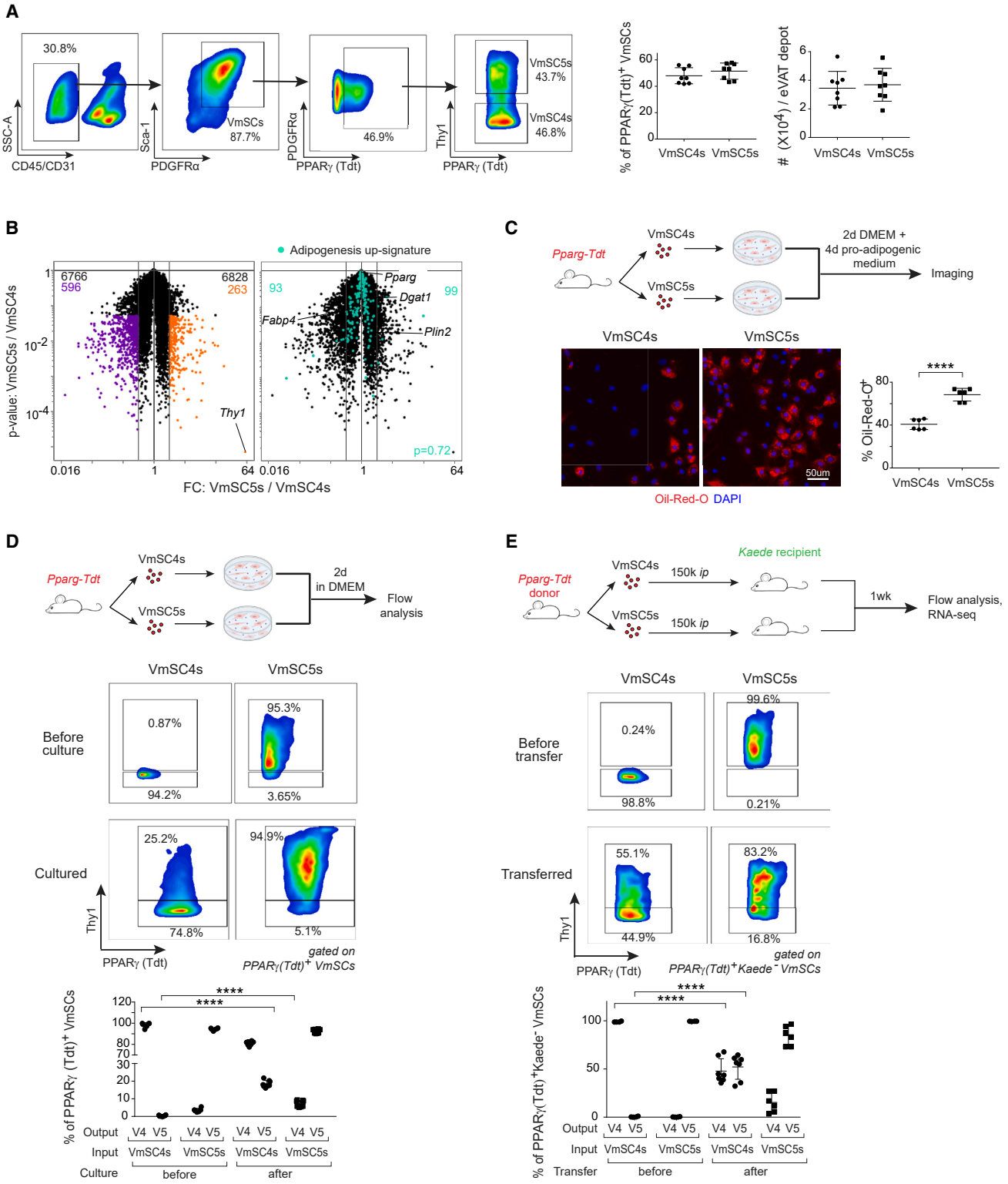

Figure 1. VmSC4s include precursors of VmSC5s but not vice versa

(A) Representative gating strategy for analyzing VmSC4s and 5s (left); summary quantification of their percentages and numbers (right). $n = 8$.

(B) Volcano plot showing genes differentially expressed (fold-change [FC] > 2, $p < 0.05$) by freshly isolated VmSC4s and 5s (left). Transcripts from an adipogenesis up-signature[23] are highlighted on the volcano plot in cyan (right). Triplicate data.

(legend continued on next page)

Please cite this article in press as: Wang et al., Adipose-tissue Treg cells restrain differentiation of stromal adipocyte precursors to promote insulin sensitivity and metabolic homeostasis, Immunity (2024), https://doi.org/10.1016/j.immuni.2024.04.002

VmSC subtypes (4 and 5) are capable of engendering adipocytes according to *in vitro* adipogenesis assays. The other three subtypes (1–3) can modulate immunocyte activities by producing growth or survival factors such as IL-33, important for both Treg cell and ILC2 accumulation and function.[15,16] There is evidence of two-way crosstalk between the immunocyte-promoting mSCs and Treg cells in VAT: VmSCs 1–3 are the major eVAT cell type producing IL-33, which is a potent inducer of the activation and proliferation of eVAT-Treg cells, which, in turn, inhibits production of IL-33 by VmSCs 1–3.[15]

The observation that eVAT-Treg cells talk back to the immunocyte-promoting VmSC subtypes raises an obvious question: do eVAT-Treg cells also communicate with the adipocyte-generating VmSC subtypes? This question seems timely, given a growing body of work demonstrating that tissue Treg cells can influence the proliferation, differentiation, and even fate choice of parenchymal cell precursors in the local microenvironment.[17–21] We have employed a combination of *in vitro* culture and *in vivo* transfer experiments to demonstrate that eVAT-Treg cells inhibit differentiation of the VmSC5 adipocyte-precursor population into mature adipocytes. Transcriptomic data, validated by analyses on conditionally mutant mice and their cells, revealed that signaling through the oncostatin-M receptor (OSMR) displayed on VmSCs by OSM secreted from eVAT-Treg cells was a key molecular interaction, manipulation of which had a strong impact on systemic metabolic tenor. These findings have uncovered an additional mechanism by which eVAT-Treg cells can regulate insulin sensitivity and related metabolic indices.

RESULTS

The VmSC4 population includes precursors of VmSC5s

As a prelude to the Treg studies, we addressed the relationship between VmSC4s and VmSC5s. We identified VmSCs by flow cytometry as CD45$^-$CD31$^-$Sca-1$^+$PDGFRα^+ cells, exploited cells from *Pparg-Tdtomato(Tdt)*-reporter mice[22] to distinguish adipogenic VmSCs 4 and 5 from immunomodulatory VmSCs 1–3, and relied on anti-Thy1 staining to separate VmSC4s from VmSC5s (Figure 1A, left). The eVAT depot of lean 16-week-old C57BL/6 (B6) mice harbored approximately equal numbers of VmSC4s (PPARγ^+Thy1$^-$) and VmSC5s (PPARγ^+Thy1$^+$) (Figure 1A, right).

We performed transcriptional analyses and *in vitro* adipogenesis assays to compare the adipogenic potential of the two stromal cell subtypes. Population-level RNA sequencing (RNA-seq) on cytofluorimetrically sorted cells revealed 859 transcripts differentially expressed in VmSCs4s and VmSC5s (at an arbitrary cut-off of 2-fold and $p \leq 0.05$) (Figure 1B). An adipogenesis signature[23]—including standard adipocyte markers such as *Pparg*, *Fabp4*, *Plin2*, and *Dgat1*—partitioned essentially equally between the two VmSC subtypes. Nonetheless, the sorted VmSC5 population gave rise to more oil red O$^+$ mature adipocytes than did VmSC4s in a standard *in vitro* adipogenesis assay (Figure 1C). Because mature adipocytes are known to be heterogeneous,[7,24] we extended the culture duration to 8 days to ensure complete differentiation and performed population-level RNA-seq to compare the transcriptomes of the resulting cells. Adipocytes engendered from cytofluorimetrically sorted VmSCs 4 and 5 were transcriptionally very similar (only 92 genes differentially expressed $\geq$2-fold, $p \leq 0.05$) (Figure S1A), suggesting that these two VmSC subtypes were more likely to represent different stages than different pathways of differentiation.

To directly address the precursor:product relationship between VmSCs 4 and 5, we examined their interconversion both *in vitro* and *in vivo*. Culturing the sorted PPARγ^+Thy1$^-$ VmSC4 population *in vitro* for 2 days led to a substantial increase in the fraction of Thy1$^+$ cells, while parallel culture of PPARγ^+Thy1$^+$ VmSC5s did not give rise to additional Thy1$^-$ cells (Figure 1D). Likewise, adoptive transfer of sorted PPARγ^+Thy1$^-$VmSC4s into B6.*Kaede* reporter mice resulted in an even split between Thy1$^-$ and Thy1$^+$ transferred cells, while adoptively transferred Thy1$^+$ VmSC5s remained almost entirely Thy1$^+$ (Figure 1E). To rule out the possibility that the Thy1$^+$ cells engendered by transfer of sorted VmSC4s merely reflected upregulation of Thy1, we retrieved the Thy1$^-$ and Thy1$^+$ cells that arose after introduction of VmSC4s and performed population-level RNA-seq. The Thy1$^+$ cells showed an enrichment in the great majority of transcripts shown in Figure 1B to distinguish the VmSC4 and 5 subtypes (Figure S1B).

Clearly, then, the VmSC4 population included cells that could give rise to VmSC5s. However, the VmSC5 population did not engender significant numbers of VmSC4s.

Treg cells regulate the accumulation of VmSC5s

To address whether eVAT-Treg cells regulate the activities of adipocyte-precursor cells, we took a genetic loss-of-function approach. In general, strategies to genetically ablate mouse Treg cells entail organism-wide depletion, which can often confound data interpretation due to the induction of systemic inflammation. However, two features of eVAT-Treg biology permit more specific ablation that, in particular, leaves lymphoid-organ Treg compartments intact: restriction of eVAT-Treg generation to the first few weeks of life[25] and their unusual dependence on PPARγ for accumulation and function.[10] We exploited each of these features in loss-of-function studies.

First, we depleted Treg cells for 3 days in 12-week-old B6.*Pparg-Tdt.Foxp3-Dtr* (hereafter DTR$^+$) mice via treatment

(C) Freshly isolated VmSC4s or 5s from 12-week-old *Pparg-Tdt* mice were cultured in DMEM for 2 days, then switched to pro-adipogenic medium for 4 days, followed by oil red O staining (blue = DAPI, red = oil red O); right: summary quantification. $n = 6$.
(D) Freshly isolated VmSC4s or 5s from 12-week-old *Pparg-Tdt* mice were cultured in DMEM for 2 days, followed by flow-cytometric analysis. Top: experimental scheme; left four panels: representative staining profiles; right panel: summary data. $n = 6$.
(E) Freshly isolated VmSC4s or 5s from 12-week-old *Pparg-Tdt* mice were i.p. injected into 10-week-old B6.*Kaeda* recipient mice, which were sacrificed 1 week after injection and analyzed by flow cytometry. Top panel: experimental scheme; left four panels: representative staining profiles; right panel: summary data. $n = 7, 6$.
V, VmSC; DMEM, Dulbecco's modified Eagle's medium.
Mean ± SD. **** $p < 0.0001$.

Please cite this article in press as: Wang et al., Adipose-tissue Treg cells restrain differentiation of stromal adipocyte precursors to promote insulin sensitivity and metabolic homeostasis, Immunity (2024), https://doi.org/10.1016/j.immuni.2024.04.002

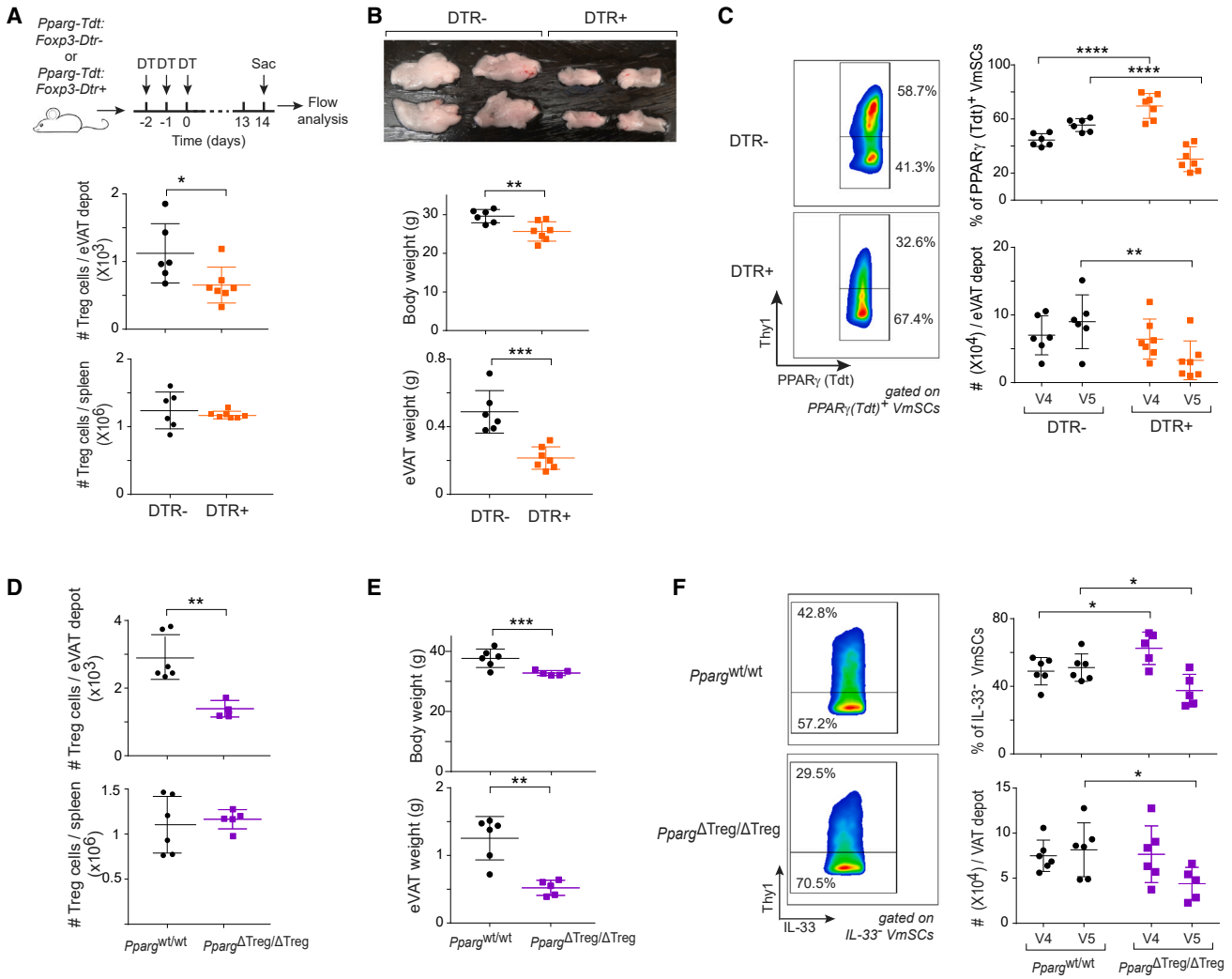

Figure 2. eVAT-Treg cells promote accumulation of VmSC5s

(A–C) 12-week-old *Foxp3-Dtr*$^{-}$ ($n = 6$) or *Foxp3-Dtr*$^{+}$ ($n = 7$) littermates were i.p. injected with 3 doses of diphtheria toxin (DT) and sacrificed at 14 days after the last injection.

(A) Top: experimental scheme; bottom: total Treg cell numbers in eVAT (left) or spleen (right).

(B) Top: representative eVAT images from DT-treated *Foxp3-Dtr*$^{-}$ or *Foxp3-Dtr*$^{+}$ littermates; bottom: quantification of body (left) and eVAT (right) weights.

(C) Flow-cytometric analysis of VmSC4s and 5s from the mice of (A). Left pair of panels: representative staining profiles; right pair: summary data for cell fractions and numbers.

(D–F) 16-week-old *Pparg*$^{wt/wt}$ ($n = 6$) and *Pparg*$^{\Delta Treg/\Delta Treg}$ ($n = 5$) littermates were sacrificed, and single-cell suspensions of eVAT analyzed by flow cytometry.

(D) Summary data on total Treg cells from eVAT (upper) or spleen (lower).

(E) Quantification of body (upper) or eVAT (lower) weights.

(F) Flow-cytometric analysis of VmSC4s and 5s from the mice of (D). Left pair of panels: representative staining profiles; right pair: summary quantification of all fractions and numbers.

DT, diphtheria toxin; V, VmSC.

Mean ± SD. * $p < 0.05$, ** $p < 0.01$, *** $p < 0.001$, and **** $p < 0.0001$.

with diphtheria toxin (DT) and allowed them to reconstitute for 2 weeks in the absence of DT (Figure 2A, upper panel). Negative controls were DT-treated littermates that did not express the DT receptor (hereafter DTR^{-}). Consistently, and as expected,[8,25] this protocol resulted in a strong reduction in eVAT-, but not spleen-, Treg cells in DTR^{+}, but not DTR^{-}, mice (Figure 2A, lower panels). There was a significant reduction in body weight as well as a >50% decrease in eVAT weight upon loss of Treg cells in DTR^{+} compared with DTR^{-} mice (Figure 2B). Flow cytometric analysis of the adipogenic (i.e., PPARγ^{+}) stromal cell subtypes, VmSCs 4 and 5, revealed a shift in their ratio due to a loss of VmSC5s (Figure 2C).

Second, we examined eVAT of 16-week-old mice lacking PPARγ expression specifically in Treg cells, i.e., in *Foxp3-Cre.P-parg*$^{fl/fl}$ mice (hereafter *Pparg*$^{\Delta Treg/\Delta Treg}$), which were previously reported to lack most Treg cells in eVAT but not in other tissues[10] (confirmed in Figure 2D). Again, body and eVAT weights were lower in mutant than in wild-type mice (Figure 2E). And, again,

Please cite this article in press as: Wang et al., Adipose-tissue Treg cells restrain differentiation of stromal adipocyte precursors to promote insulin sensitivity and metabolic homeostasis, Immunity (2024), https://doi.org/10.1016/j.immuni.2024.04.002

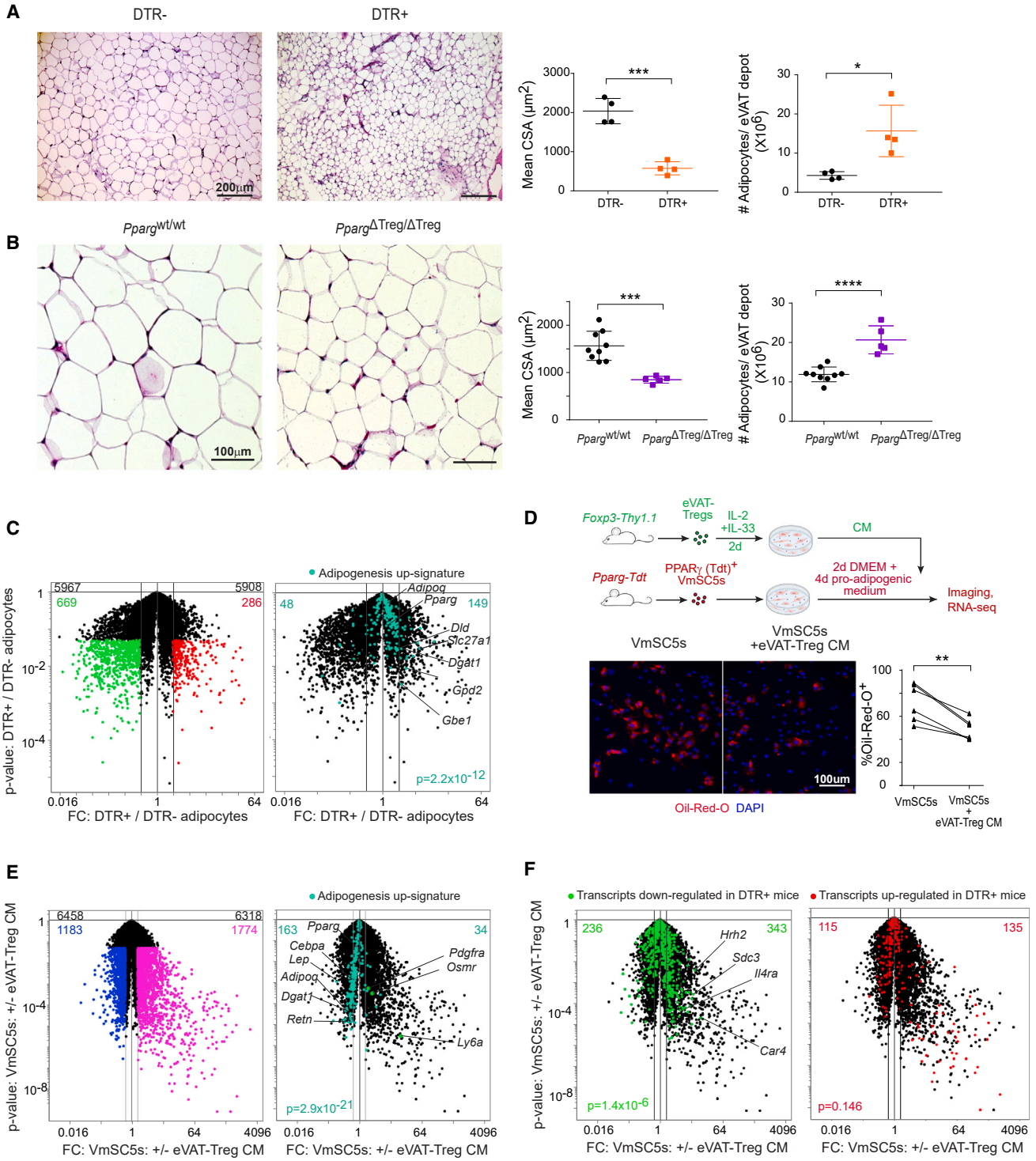

Figure 3. eVAT-Treg cells promote VmSC5 accumulation by directly suppressing their further differentiation

(A) Left pair of panels: H&E staining of eVAT sections from 12-week-old *Foxp3-Dtr*$^{-}$ ($n = 4$) or *Foxp3-Dtr*$^{+}$ ($n = 4$) littermates depleted of Treg cells as per Figure 2A; right pair of panels: quantification of adipocyte mean cross-sectional areas (left) or numbers (right).

(B) Same as the (A), except 16-week-old *Pparg*$^{wt/wt}$ ($n = 9$) and *Pparg*$^{\Delta Treg/\Delta Treg}$ ($n = 5$) littermates were compared.

(C) Volcano plot showing transcripts differentially expressed (FC > 2, $p < 0.05$) in floating adipocytes of DT-treated *Foxp3-Dtr*$^{-}$ vs. *Foxp3-Dtr*$^{+}$ littermates (as per Figure 2A, left). Transcripts from an adipogenesis up-signature[23] are highlighted in cyan (right). Duplicate samples.

(legend continued on next page)

Please cite this article in press as: Wang et al., Adipose-tissue Treg cells restrain differentiation of stromal adipocyte precursors to promote insulin sensitivity and metabolic homeostasis, Immunity (2024), https://doi.org/10.1016/j.immuni.2024.04.002

mice lacking Treg cells in eVAT showed a paucity of VmSC5s but not VmSC4s (Figure 2F) (note that for these mice, adipogenic VmSCs were delineated as IL-33$^-$, as per Spallanzani et al.[15]).

Thus, eVAT-Treg cells positively impacted the accumulation of VmSC5s but not VmSC4s. This effect appeared not to emanate from systemic inflammation.

eVAT-Treg cells foster VmSC5 accumulation via direct suppression of their differentiation into adipocytes

Cell compartment sizes can be regulated by several processes: input from a less mature stage, proliferation, death, or output to a more mature stage. To examine the impact of eVAT-Treg cells on progression from the less mature VmSC4 to the more mature VmSC5 compartment, we intraperitoneally (i.p.) transferred cytofluorimetrically sorted, Tdt-labeled VmSC4s into DT-treated DTR$^-$ (control) and DTR$^+$ (Treg-deficient) recipients, then waited 1 week for them to install and differentiate. The efficiency of VmSC4 differentiation into VmSC5s was equally effective in the presence or absence of Treg cells in the recipient mice (Figure S2A). Nor was there a difference in the fraction of VmSC5s in cycle (Ki67$^+$) (Figure S2B) or undergoing apoptosis (Annexin-5$^+$) (Figure S2C) in straight DT-treated DTR$^+$ vs. DTR$^-$ mice. By contrast, there was a striking disparity in progression from the VmSC5 compartment to the mature adipocyte stage in mice with or without Treg cells. Hematoxylin and eosin (H&E)-stained sections of eVAT revealed there to be substantially more and smaller adipocytes in the eVAT depots of DT-treated DTR$^+$ (Figure 3A) and *Pparg*$^{\Delta Treg/\Delta Treg}$ (Figure 3B) mice, each deficient in eVAT-Treg cells, compared with their control littermates. As the >2-fold increase in adipocyte numbers in the two models was suggestive of *de novo* adipogenesis, we performed RNA-seq on floating adipocytes from DT-treated DTR$^-$ and DTR$^+$ littermates to evaluate this notion. There was indeed enrichment of the classic adipogenesis signature—including higher expression of *Gbe1*, *Gpd2*, and *Dgat1*—in adipocytes from DTR$^+$ mice (Figure 3C).

To ascertain whether eVAT-Treg cells inhibited adipogenesis directly or indirectly, we co-cultured VmSC5s under adipogenic conditions in the presence or absence of conditioned medium (CM) from eVAT-Treg cells. *In vitro* differentiation of VmSC5s into mature adipocytes was significantly inhibited by soluble factors produced by eVAT-Treg cells (Figure 3D), while CM from spleen Treg cells stimulated only with IL-2 had no such effect (Figure S3). However, CM from splenic Treg cells exposed to IL-2 plus IL-33 effectively suppressed the differentiation of VmSC5s to adipocytes (Figure S3). To rule out the possibility that fewer oil red O$^+$ cells merely reflected a defect in lipid metabolism, we performed RNA-seq on end-point cells from the cultures, with and without CM from eVAT-Treg cells, which demonstrated abundant transcriptional differences (Figure 3E, left). Consistent with the *in vivo* data in Figure 3C, expression of adipogenesis signature genes like *Lep*, *Adipoq*, *Dgat1*, and *Retn* was reduced in VmSC5s differentiated in the presence of CM; on the contrary, markers of adipocyte-precursor cells—notably *Pdgfra* and *Ly6a* transcripts—were maintained in the presence of CM, pointing to a block in adipogenesis (Figure 3E, right). Of the 669 genes transcribed less strongly in *ex vivo* adipocytes from DT-treated DTR$^+$ mice (fluo-green-highlighted data from Figure 3C), expression of over half of them (343) was increased $\geq$2-fold by addition of eVAT-Treg CM to adipogenic cultures of VmSC5s (Figure 3F, left). Likewise, 46% of the genes transcribed more strongly in *ex vivo* adipocytes from DT-treated DTR$^+$ mice (fluo-red-highlighted data from Figure 3C) showed decreased expression in the presence of eVAT-Treg CM (115 of 250) (Figure 3F, right), indicating that many of the transcriptomic changes induced by eVAT-Treg cells were direct.

In brief, then, the positive impact of eVAT-Treg cells on VmSC5 accumulation reflected their inhibition of VmSC5 differentiation into mature adipocytes. This control issued from a direct effect of one or more soluble mediators produced by Treg cells.

eVAT-Treg cells limit adipogenesis through oncostatin M (OSM)

As a first step in identifying the key inhibitory mediator(s) produced by eVAT-Treg cells, we performed pathway enrichment analysis on the transcripts differentially expressed by VmSC5s matured in the presence vs. absence of CM from eVAT-Treg cells (pink-highlighted transcripts in Figure 3E). Several cytokine-signaling pathways—notably, the IL-2, IL-1, TGF-β, OSM, and IFN pathways—were strengthened by the addition of CM (Figure 4A). Because OSM is known to inhibit the differentiation of 3T3-L1 cells or mouse embryonic fibroblasts into adipocytes,[26] our attention was first drawn to this pathway. Importantly, published transcriptomic data[22] revealed more *Osm* transcripts in eVAT-Treg, but not eVAT-nonTreg CD4$^+$, cells than in their splenic counterparts (Figure 4B, left). And the RNA-seq data illustrated in Figure 1B showed abundant *Osmrb* transcripts in both VmSC4s and 5s (Figure 4B, right); furthermore, almost all of both subtypes displayed cell-surface OSMR (Figure 4C).

To determine whether OSM is able to influence VmSC5 differentiation, we cultured cytofluorimetrically sorted VmSC5s with OSM or phosphate-buffered saline (PBS) under adipogenic conditions and compared their ability to engender mature adipocytes (Figure 4D). Although most VmSC5s differentiated into adipocytes after PBS addition, OSM supplementation completely blocked VmSC5 maturation. In addition, the adipogenesis up-signature—including *Pparg*, *Adipoq*, *Dgat1*, *Apoe*, *Fabp4*, and *Lipe*—was strongly attenuated in VmSC5s

(D) Freshly isolated VmSC5s from 12-week-old *Pparg-Tdt* mice were cultured with or without conditioned medium from eVAT-Treg cells for 2 days in DMEM, then pro-adipogenic medium for 4 days, followed by oil red O staining. Top: experimental scheme; bottom left: representative images (blue = DAPI, red = oil red O); right: summary quantification. $n = 6$.

(E) Volcano plot showing transcripts differentially expressed (FC > 2, $p < 0.05$) by adipocytes matured in culture in the presence vs. absence of conditioned medium from eVAT-Treg cells (left). Transcripts from an adipogenesis up-signature[23] are highlighted in cyan (right). Triplicate samples.

(F) Transcripts expressed less (left) or more (right) strongly in floating adipocytes from *Foxp3-Dtr*$^+$ mice compared with those of Dtr$^-$ littermates in (C) are highlighted on the volcano plot of (E).

CSA, cross-sectional area; DMEM, Dulbecco's modified Eagle's medium; and CM, conditioned medium.

Mean ± SD. *p* values as per Figure 2.

Please cite this article in press as: Wang et al., Adipose-tissue Treg cells restrain differentiation of stromal adipocyte precursors to promote insulin sensitivity and metabolic homeostasis, Immunity (2024), https://doi.org/10.1016/j.immuni.2024.04.002

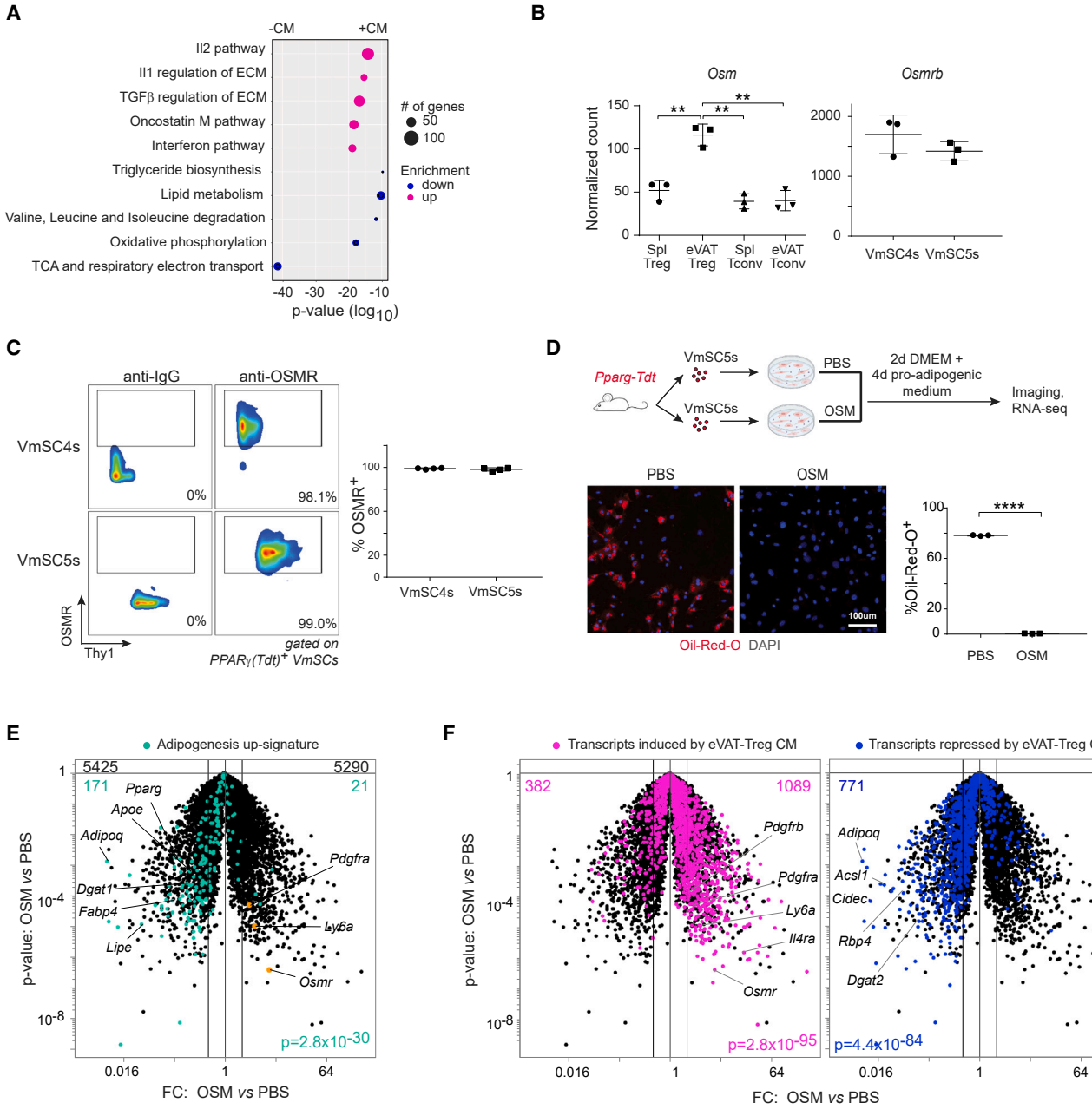

Figure 4. OSM produced by eVAT-Treg cells inhibits adipogenesis *in vitro*

(A) Pathway enrichment analysis of transcripts differentially expressed when VmSC5s mature in culture in the presence vs. absence of CM from eVAT-Treg cells (pink- and blue-colored genes in Figure 3E).

(B) Left: expression of *Osm* transcripts by splenic vs. eVAT-Treg and eVAT-Tconv cells (data from Li et al.[22]); right: expression of *Osmrb* transcripts by VmSC4s vs. 5s (data from Figure 2B).

(C) Flow-cytometric analysis of OSMR expression by freshly isolated VmSC4s and 5s. Left: representative staining profiles; right: summary data. $n = 4$.

(D) Freshly isolated VmSC5s from 12-week-old *Pparg-Tdt* mice were cultured with PBS or 10 ng/ml OSM in DMEM for 2 days, then pro-adipogenic medium for 4 days, followed by oil red O staining. Top: experimental scheme; bottom left: representative images (blue = DAPI; red = oil red O); bottom right: summary quantification. $n = 3$.

(E) An adipogenesis up-signature[23] is highlighted on a volcano plot comparing transcripts expressed by VmSC5s cultured in the presence of OSM or PBS as per (D). Triplicate samples.

(F) Same as (E), except transcripts expressed more (left) or less (right) strongly in VmSC5s cultured with eVAT-Treg CM (vs. alone) are highlighted.

PBS, phosphate-buffered saline; Tconv, conventional CD4+ T cells. Other abbreviations as per Figure 3.

Mean ± SD. *p* values as per Figure 2.

Please cite this article in press as: Wang et al., Adipose-tissue Treg cells restrain differentiation of stromal adipocyte precursors to promote insulin sensitivity and metabolic homeostasis, Immunity (2024), https://doi.org/10.1016/j.immuni.2024.04.002

differentiated in the presence of OSM; by contrast, transcripts characteristic of adipocyte precursors—like *Pdgfra* and *Ly6a*—were not reduced (Figure 4E). Notably, *Osmrb* transcripts were increased in VmSC5s by OSM, suggestive of a feed-forward loop. We then addressed the overlap between OSM- and Treg-regulated transcripts by superimposing the sets of transcripts induced or repressed by Treg cell CM ($\geq$2-fold, $p < 0.05$; pink- and blue-highlighted transcripts in Figure 3E) on the volcano plot comparing the effect of OSM and PBS on VmSC5 differentiation. The majority of transcripts induced by CM from eVAT-Treg cells were also increased by OSM (1,089 of 1,774); likewise, most of the transcripts repressed by CM from eVAT-Treg cells were decreased by OSM, at least to some degree (771 of 1,183) (Figure 4F). Thus, OSM is likely to be a major mediator of the eVAT-Treg impact on *in vitro* adipogenesis. To directly test the importance of OSM in the *in vitro* inhibition of adipocyte maturation by CM from eVAT-Treg cells, we cultured VmSC5s under adipogenic conditions with CM in the presence or absence of anti-OSM neutralizing antibodies (Abs). Consistent with the results depicted in Figure 3D, fewer mature adipocytes were generated when CM from eVAT-Treg cells was added to the adipogenic cultures, and OSM neutralization released this inhibition (Figure 5A), confirming that OSM is probably the major inhibitor of adipogenesis and thereby promoter of VmSC5 accumulation, produced by eVAT Tregs, at least *in vitro*.

To address the importance of OSM in the *in vivo* inhibition of adipocyte maturation by eVAT-Treg cells, we first estimated the degree to which loss of Treg cells (primarily in eVAT) impacted the local concentration of OSM. ELISA quantification revealed an approximately 50% and 30% reduction of the normal OSM concentration in eVAT of DT-treated DTR^{+} and *Pparg*$^{\Delta Treg/\Delta Treg}$ mice, respectively (Figure 5B)—this in the context of an approximately 40% and 50% loss of total Treg cell numbers, respectively (Figures 2A and 2D). Thus, OSM produced by Treg cells contributed a substantial fraction of the total eVAT pool of OSM. Next, we performed an *in vivo* complementation experiment by i.p. injecting PBS vs. OSM into DT-treated DTR^{-} vs. DTR^{+} littermates (Figure 5C). Consistent with the results depicted in Figure 2C, PBS-treated mice deficient in Treg cells (DT-treated DTR^{+}) had fewer VmSC5s than control (DT-treated DTR^{-}) mice had, while OSM-treated mice lacking Treg cells had about twice as many VmSC5s as their PBS-treated counterparts did. There were shifts in the VmSC4:VmSC5 ratio, but these changes reflected impacts on VmSC5s as there were no significant alterations in VmSC4 numbers in mice of the different genotypes or treatment conditions. Thus, administration of OSM to mice lacking Treg cells substantially, but not completely, complemented their reduction in VmSC5s. H&E histology revealed that injection of OSM could also complement the overexuberant adipogenesis of these mice—again, substantially though not completely (Figure 5D).

In brief, transcriptomic analyses implicated OSM signaling as a potentially important pathway in the inhibition of VmSC5 maturation into adipocytes mediated by eVAT-Treg cells. Data from *in vitro* and *in vivo* systems, entailing both gain- and loss-of-function approaches, converged to establish that OSM was a major and direct mediator of Treg cell regulation of VmSC5 differentiation.

In vivo engagement of Treg-produced OSM by mSC-displayed OSMR promotes insulin sensitivity

Additional *in vivo* support for the above-proposed scenario was provided by the phenotype of a pair of conditionally mutant mouse lines. We ablated *Osm* specifically in Treg cells by generating *Foxp3-Cre.Osm*$^{fl/fl}$ mice (hereafter *Osm*$^{\Delta Treg/\Delta Treg}$, Figure S4A). According to ELISA results, the ablation of *Osm* specifically in Treg cells resulted in an approximately 30% reduction in the total concentration of OSM in the eVAT depot (Figure S4B). Flow cytometric analysis showed the anticipated shift in the VmSC4:VmSC5 ratio due to fewer VmSC5s in *Osm*$^{\Delta Treg/\Delta Treg}$ than in *Osm*$^{wt/wt}$ mice (Figure 6A). Mimicking the findings on DT-treated DTR^{+} (Figure 2C) and *Pparg*$^{\Delta Treg/\Delta Treg}$ (Figure 2F) mice, H&E-stained histological sections revealed more and smaller adipocytes in the eVAT depot of the mutant mice than in their littermate controls (Figure 6B). Lastly, *Osm*$^{\Delta Treg/\Delta Treg}$ mice exhibited clear metabolic deficiencies: the insulin-tolerance test (ITT) showed insulin resistance (Figure 6C), while the glucose-tolerance test (GTT) indicated glucose intolerance (Figure 6D) relative to *Osm*$^{\Delta Treg/\Delta Treg}$ littermates.

Importantly, the loss of *Osm* expression by Treg cells only minimally affected the number, transcriptome, and anti-inflammatory function of Treg cells in eVAT and the spleen. There were no significant differences in the fraction or number of Treg cells in either tissue of the mutant mice vs. their wild-type littermates (Figure S4C) and only a very slight increase in the relative contribution of the ST2^{+} Treg subtype, and only in the spleen (Figure S4D). Reflective of their Tregs' anti-inflammatory capacity, *Osm*$^{\Delta Treg/\Delta Treg}$ and *Osm*$^{wt/wt}$ mice had equivalent representations of total immunocytes (Figure S4E), MFs (Figure S4F), and activated MFs (Figure S4G), true of both eVAT and the spleen. Not surprisingly, then, there were only very mild transcriptional differences between the Treg compartments of the wild-type and mutant mice Figure S4H). Moreover, pathway analysis of the genes with increased or decreased expression (fold-change [FC] > 2; $p < 0.01$) using multiple programs revealed no significant pathways, and a large fraction of these genes had uncharacterized "GM" designations.

We also ablated *Osmrb* in mSCs by generating *Pdgfra-Cre.Osmrb*$^{fl/fl}$ mice (hereafter *Osmrb*$^{\Delta mSC/\Delta mSC}$) (and littermate controls) (Figure S4I). Analogous studies on these mutants yielded results strikingly parallel to those on the *Osm*$^{\Delta Treg/\Delta Treg}$ mutants: fewer VmSC5s (Figure 6E), more and smaller adipocytes (Figure 6F), and insulin resistance coupled with glucose intolerance (Figures 6G and 6H) vis-à-vis littermate controls.

Because mice lacking OSMR on cells expressing the *Adipoq* gene (assumed to be mature adipocytes) have been reported to exhibit metabolic abnormalities,[27,28] and because VmSC5s showed some *Adipoq* expression (e.g., Figures 3E and 4E), we wondered to what extent the previously published metabolic phenotypes might reflect an impact on VmSC5 differentiation into mature adipocytes. Therefore, we also produced *Adipoq-Cre.Osmrb*$^{fl/fl}$ mice (hereafter *Osmrb*$^{\Delta Ad/Ad}$) and littermate controls. Loss of OSMR from *Adipoq*$^{+}$ cells resulted in insulin resistance and glucose intolerance, but both deficiencies were much milder than what we saw in mice lacking OSMR on *Pdgfra*$^{+}$ cells (compare Figure S5A with Figure 6G and Figure S5B with Figure 6H). We did not, however, see changes in adipocyte size or

Please cite this article in press as: Wang et al., Adipose-tissue Treg cells restrain differentiation of stromal adipocyte precursors to promote insulin sensitivity and metabolic homeostasis, Immunity (2024), https://doi.org/10.1016/j.immuni.2024.04.002

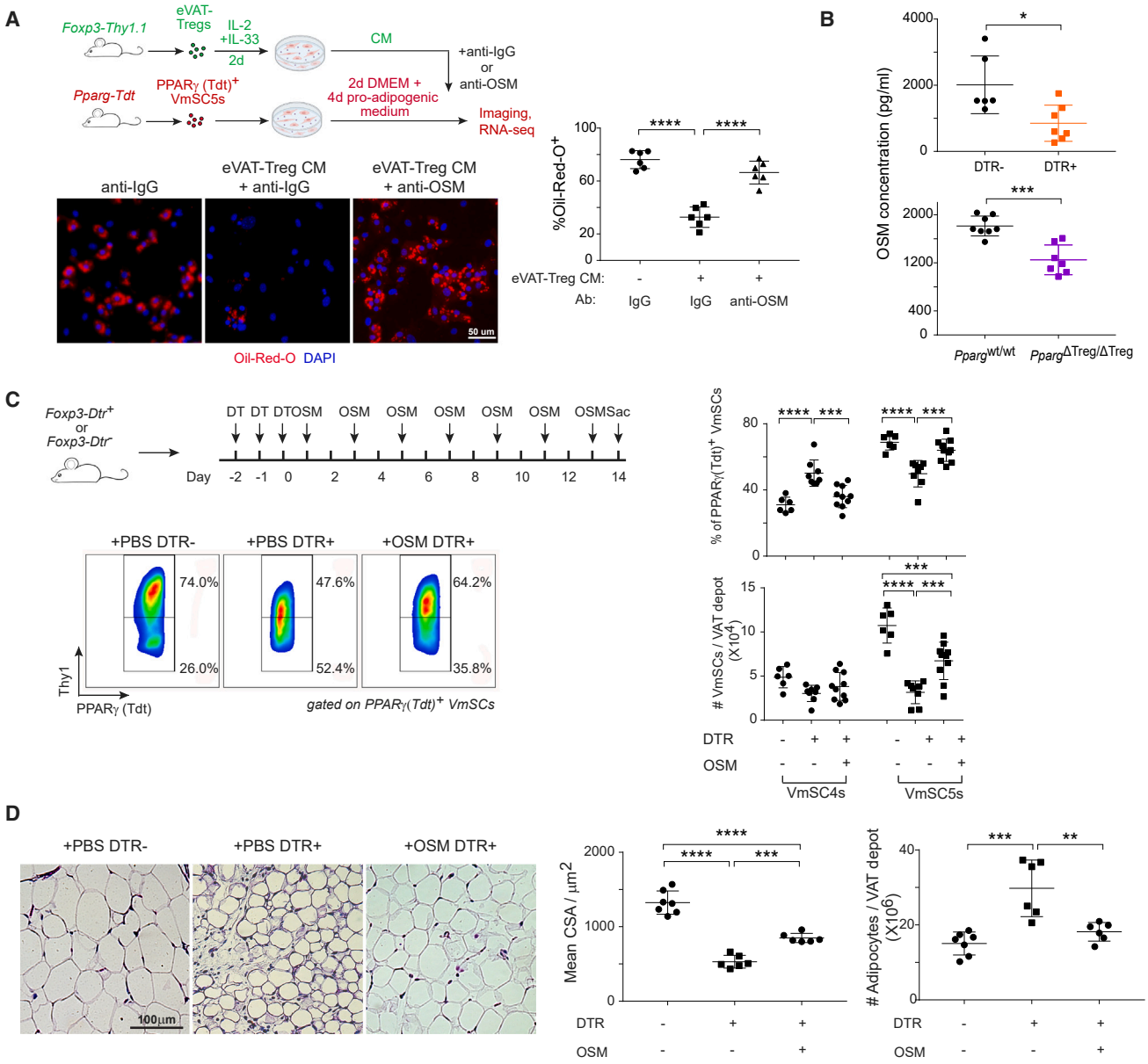

Figure 5. *In vivo* administration of OSM rescues VmSC5s in mice lacking Treg cells

(A) Freshly isolated VmSC5s from 12-week-old *Pparg-Tdt* mice were cultured with or without CM from eVAT-Treg cells in combination with either anti-OSM antibodies or control IgG in DMEM for 2 days, then in pro-adipogenic medium for 4 days (+Abs), followed by oil red O staining. Top: experimental scheme; bottom: imaging (blue = DAPI, red = oil red O); right: summary quantification. $n = 6$.

(B) ELISA measurements of OSM concentrations in eVAT interstitial fluid of *Foxp3-Dtr*$^{-}$ ($n = 6$) or *Foxp3-Dtr*$^{+}$ ($n = 7$) littermates (upper) and of *Pparg*$^{wt/wt}$ ($n = 8$) or *Pparg*$^{\Delta Treg/\Delta Treg}$ ($n = 7$) littermates (lower).

(C–D) 12-week-old *Foxp3-Dtr*$^{-}$ or *Foxp3-Dtr*$^{+}$ littermates were i.p. injected with DT daily for 3 days, followed by OSM (40 ng/g body weight) every other day, and were sacrificed 14 days after the last DT injection. $n = 6$–10.

(C) Top: experimental scheme; bottom: representative cytofluorimetric profiles; right: summary quantification of the fraction (upper) and number (lower) of VmSC4s and 5s.

(D) Left panels: H&E staining of eVAT sections. Right panels: quantification of mean CSA and adipocyte numbers.

DT, diphtheria toxin; other abbreviations as per Figure 3.

Mean ± SD. *p* values as per Figure 2.

number in *Osmrb*$^{\Delta Ad/Ad}$ mice (Figure S5C), indicating that the metabolic phenotype of these mice clearly had a different provenance.

Thus, *in vivo* engagement of Treg-produced OSM by mSC-displayed OSMR promoted the accumulation of VmSC5s by inhibiting their differentiation into mature adipocytes. Breaking

Please cite this article in press as: Wang et al., Adipose-tissue Treg cells restrain differentiation of stromal adipocyte precursors to promote insulin sensitivity and metabolic homeostasis, Immunity (2024), https://doi.org/10.1016/j.immuni.2024.04.002

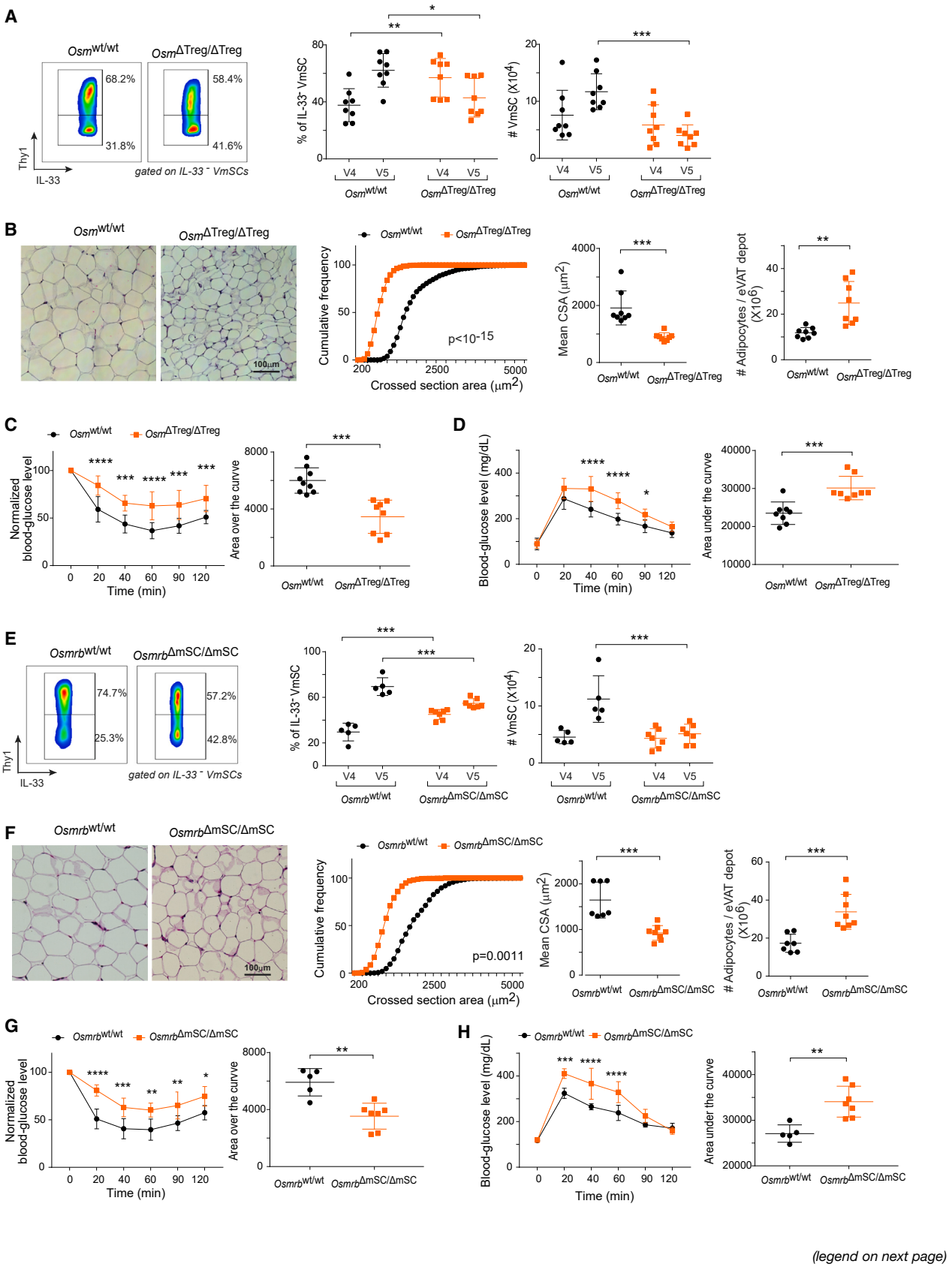

(legend on next page)

off these engagements resulted in deficiencies in systemic metabolism.

The OSM:OSMR axis is conserved in humans

Re-analysis of published datasets allowed us to evaluate the potential of human eVAT-stromal cells to respond to eVAT-Treg cells. Recent scRNA-seq data on human VAT from control non-cachectic cancer patients[29] revealed that *OSMRB*-expressing cells were largely confined to *PDGFRA*$^{+}$ VmSC cell clusters (Figure 7A). Focusing specifically on the PDGFRA^{+} cells, we found that, just as in mice, there was extensive overlap between cells expressing *PPARG*, i.e., the adipocyte-precursor cells, and those expressing *OSMRB* (Figure 7B). The mouse:human correspondence was even more profound, as the human homologs of the mouse transcripts whose expression best correlated with that of *Osmrb* in murine VmSCs strongly overlapped with *OSMRB* expression in human VmSCs (Figure 7C). As illustrated in Figure 4B, murine adipose tissue Treg cells expressed more than double the number of *Osm* transcripts than splenic Treg cells did. Similarly, human adipose tissue Treg cells expressed many more *OSM* transcripts than did peripheral-blood Treg cells, whether of naive or memory phenotype (Figure 7D). Thus, the Treg-cell:mSC axis of *Osm:Osmrb* expression in mouse eVAT seems to be conserved in human VAT.

DISCUSSION

eVAT-Treg cells were discovered to regulate local and systemic metabolism almost 15 years ago.[8] Much of their influence was thought to emanate from the control of eVAT inflammation—in response to genetically or nutritionally induced obesity, for example. Here, we report that eVAT-Treg cells have an additional function important for maintaining steady-state metabolism: regulation of the differentiation of mature adipocytes from precursor cells residing in the stroma. Mechanistically, this function was primarily attributed to OSM produced by eVAT-Treg cells, which signaled through OSMR displayed on stromal adipocyte precursors.

We found the insulin resistance of mice with a reduced eVAT-Treg compartment to be associated with more, smaller adipocytes. This observation appears to contrast with the insufficient adipogenesis and adipocyte hypertrophy typical of the insulin-resistant state induced by obesity.[32] Actually, very small adipocytes akin to those we found (of diameter <35 μm) were observed in mammals by histology and electron microscopy as early as the 1970s[33–35] and, with the advent of flow cytometry, it became clear that both VAT and subcutaneous adipose tissue (SAT) normally contain a bimodal distribution of adipocyte sizes.[36–38] The mean adipocyte size does increase in obese mice and humans, but it is rather the proportion of very small adipocytes in both VAT and SAT that positively correlates with insulin resistance.[39–41] Similarly, small adipocytes are enriched in mouse models of lipodystrophy, such as in mice with a *Cav1*- or *Agpat2*-null mutation[42] or with cancer cachexia.[43] Thus, limiting the accumulation of these dysfunctional small adipocytes, as eVAT-Treg cells do, should be beneficial for the maintenance of metabolic health. In addition, the smaller eVAT weight in mice deficient in local Treg cells suggests an accelerated basal lipolysis at steady state, which could cause ectopic lipid storage in skeletal muscle and the liver, thereby promoting lipotoxicity and insulin resistance. Relatedly, we recently reported that eVAT-Treg cells can suppress adipocyte lipolysis, overriding its typical circadian rhythm.[44] Lastly, it is possible that lipolysis induced by residual inflammation contributes to insulin resistance, whether associated with the very small or larger adipocytes.

Although the role of OSM in VAT processes has been studied by multiple approaches,[45] our studies highlighted another axis: OSM:OSMR-dependent, Treg-cell:adipocyte-precursor interactions. Whole-body ablation of OSM resulted in early-onset glucose intolerance upon high-fat diet (HFD) challenge, an abnormality that mapped to loss of OSM production by the hematopoietic cell compartment.[46] The culprit OSM-producing cell type has not been further delineated, with the common assumption that it is a myeloid cell (e.g., Sanchez-Infantes and Stephens[45] and Albiero et al.[46]). Our data emphasized the importance of OSM production by Treg cells in enforcing eVAT metabolic homeostasis at steady state.

Several studies examining the effects of a deficiency in OSMRβ (the unique subunit of the murine OSM receptor) have been published over the past decade. Whether the *OSMRB* gene was mutated systemically[47–49] or only in adipocytes (via an *Adipoq* driver),[27,28] and whether lean or obese mice were examined, inflammation was always more pronounced in mutant than in wild-type mice. Metabolic dysregulation (insulin resistance, glucose intolerance) was largely confined to obese mice in adipocyte-specific mutants, while it manifested more strongly and in both lean and obese mice in whole-body mutants, indicating that eVAT cells other than adipocytes are important for maintaining metabolic homeostasis, especially at steady state. Our data demonstrated a critical role for OSMRβ^{+}PDGFRα^{+} stromal cells, most likely adipocyte-generating VmSCs.

How might OSM be inhibiting the differentiation of VmSC5s into mature adipocytes? Given that VmSCs 4 and 5 are both post-mitotic adipocyte-precursor cells, we did not need to unravel influences on differentiation vs. proliferation, which can be difficult. OSM dampens adipogenesis of 3T3-L1 cells and mouse embryo fibroblasts via the Ras/ERK and STAT5 signaling

Figure 6. The OSM/OSMR axis promotes VmSC5 accumulation and insulin sensitivity

(A–D) Data from 12-week-old *Osm*$^{wt/wt}$ (n = 8) and *Osm*$^{\Delta Treg/\Delta Treg}$ (n = 8) littermates.

(A) Flow-cytometric analysis of VmSCs. Left: representative profiles; right: summary data on fraction and number of VmSC4s and 5s.

(B) H&E staining of eVAT sections (left); quantification of mean CSA and adipocyte numbers (right).

(C) Insulin-tolerance test. Left: temporal values; right: summary areas over the curve.

(D) Glucose-tolerance test. Left: temporal values; right: summary areas under the curve.

(E–H) The same as (A)–(D), except the data are from *Osmrb*$^{wt/wt}$ (n = 5) and *Osmrb*$^{\Delta mSC/\Delta mSC}$ (n = 7) littermates.

V, VmSC; otherwise, abbreviations as per Figure 2.

Mean ± SD. p values as per Figure 2.

Please cite this article in press as: Wang et al., Adipose-tissue Treg cells restrain differentiation of stromal adipocyte precursors to promote insulin sensitivity and metabolic homeostasis, Immunity (2024), https://doi.org/10.1016/j.immuni.2024.04.002

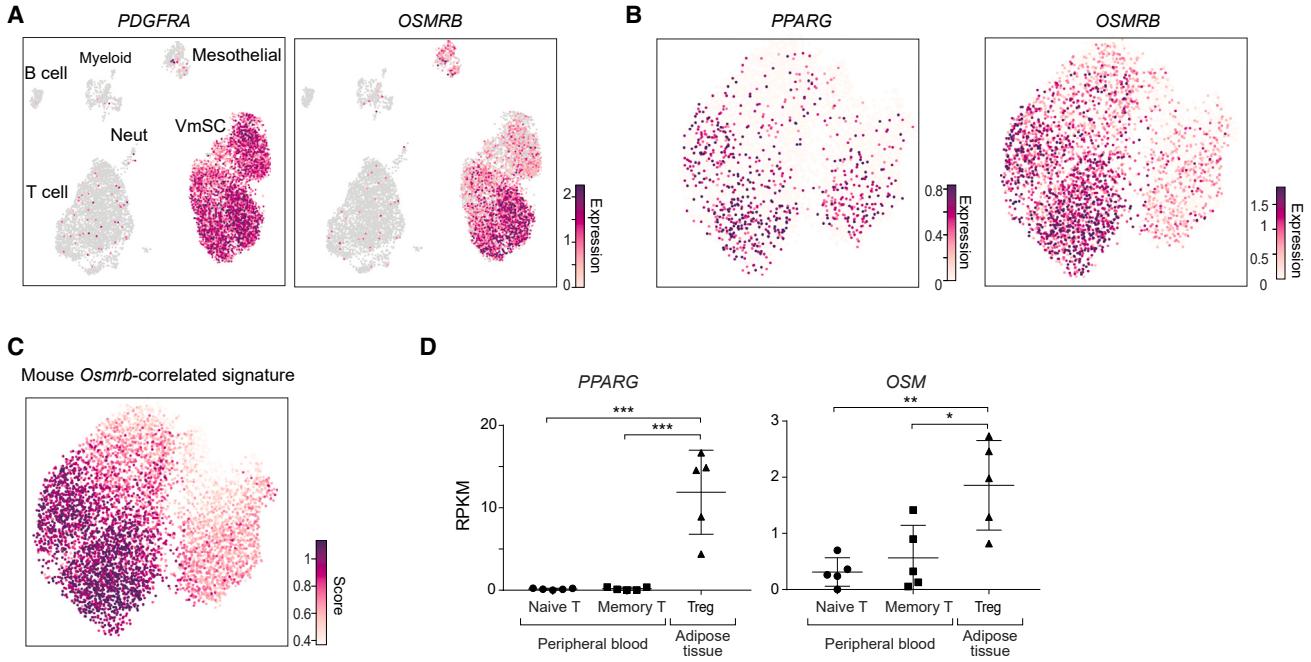

Figure 7. Conservation of the OSM/OSMR axis in human VAT

(A) Expressions of *PDGFRA* and *OSMRB* transcripts in human VAT.

(B) Expressions of *OSMRB* and *PPARG* transcripts in human VmSCs re-clustered from (A).

(C) Top 50 *Osmrb*-correlated genes extracted from mouse VmSCs (data from Yang et al.[30]) were shown in UMAP from (B).

(D) Expressions of *PPARG* and *OSM* transcripts in human Treg cells from populational-level RNA-seq (data from Delacher et al.[31]).

RPKM: reads per kilobase of transcript, per million mapped reads; UMAP, Uniform Manifold Approximation and Projection.

Mean ± SD. *p* values as per Figure 2.

pathways.[26] Further downstream, it almost totally abolishes expression of PPARγ and C/EBPα, both TFs being essential for adipogenesis. Indeed, we found both *Pparg* and *Cebpa* expression by VmSC5s to be dampened in the presence of eVAT-Treg cells (or CM from them) and by OSM.

That eVAT-Treg cells can control the activities of adipocyte-precursor cells falls under an emerging theme in Treg cell biology.[9] For example, Treg cells in injured skeletal muscle directly regulate myocyte differentiation by producing amphiregulin that binds to the epidermal growth factor receptor on muscle satellite cells,[17] and can also indirectly regulate myocyte differentiation by reining in IL-17A production.[50] Through Jagged1:Notch interactions, skin Treg cells control the hair follicle cycle by driving the division and differentiation of hair follicle stem cells.[18] In addition, intestinal Treg cells exploit IL-10 to support renewal of local stem cells, restraining their proliferation and any aberrant differentiation.[19] This Treg cell function might be a primordial one. In zebrafish, Foxp3^{+} T cells infiltrate damaged tissues, such as the spinal cord, brain, retina, and caudal fin; these cells promote tissue regeneration by secreting tissue-specific regulators of progenitor cell proliferation.[20,51] Taken together, these reports indicate that tissue Treg cells have the potential to regulate the proliferation, differentiation, or fate choice of local progenitor cells.

Limitations of the study

(1) Given the tools available, it is usually very difficult to distinguish local influences of Treg cells, such as those we have highlighted here, from their systemic effects. However, the eVAT-Treg context offers several features that allowed us to side-step this sticky issue: very preferential depletion due to the poor replenishment of eVAT-Treg cells in adult mice, highly preferential ablation in mice with a Treg-specific *Pparg*-null mutation, and performant *in vivo* adoptive transfer and *in vitro* culture systems. Thus, we were able to distill local Treg-cell:adipocyte-precursor interactions in mice at steady state. (2) Although our study demonstrated an important role for OSM:OSMR interactions in regulating adipocyte differentiation from stromal precursors, it remains possible that other Treg cell mediators are also involved. (3) We illustrated parallels in OSM and OSMR expression in human Tregs and stromal cells, but it remains to be seen how analogously this pathway operates in the control of adipogenesis.

Overall, our findings draw attention to the sophisticated armamentarium that tissue-Treg cells—in this case, eVAT-Treg cells—exploit to guard tissue homeostasis. And argue that optimal Treg-based therapies will entail more than just delivery of an anti-inflammatory cytokine. Perhaps evolution has already provided us with the best therapeutic option—tissue Treg cells themselves.

STAR★METHODS

Detailed methods are provided in the online version of this paper and include the following:

- KEY RESOURCES TABLE

- RESOURCE AVAILABILITY
  - Lead contact
  - Materials availability
  - Data availability
- EXPERIMENTAL MODEL AND PARTICIPANT DETAILS
  - Mouse models
- METHOD DETAILS
  - Animal treatment
  - Cell isolation and flow cytometry
  - Cell culture and adipogenesis assay
  - Histology
  - ITTs and GTTs
  - Quantification of gene expression by RT-qPCR
  - Bulk RNA-seq library preparation and data analysis
  - scRNA-seq analysis
- QUANTIFICATION AND STATISTICAL ANALYSIS

SUPPLEMENTAL INFORMATION

Supplemental information can be found online at https://doi.org/10.1016/j.immuni.2024.04.002.

ACKNOWLEDGMENTS

We thank K. Hattori, A. Ortiz-Lopez, T. Xiao, and N. Zammit for experimental assistance; L. Yang for bioinformatics; C. Laplace for graphics; P.K. Langston, B.S. Hanna, M. Marin-Rodero, and D. Owen for helpful discussions; the Harvard Medical School (HMS) Rodent Histopathology Core; the HMS Immunology Department Flow-Cytometry Core; and the HMS MiCRoN Core. This work was funded by grants from the NIH (2R01 DK092541), the JPB Foundation, a Dean's Innovation Grant in the Basic and Social Sciences from Harvard Medical School, and a postdoctoral fellowship (for G.W.) from Novo Nordisk.

AUTHOR CONTRIBUTIONS

G.W. and R.G.S. performed experiments. G.W. and A.R.M.-R. analyzed and interpreted data. G.W. and D.M. designed all of the experiments and wrote the manuscript, which all authors reviewed. R.A.F. provided advice and the *B6.Osm-flox* mice. C.B. and D.M. provided supervision. D.M. acquired funding.

DECLARATION OF INTERESTS

The authors declare no competing interests.

Received: May 23, 2023
Revised: February 8, 2024
Accepted: April 4, 2024
Published: April 30, 2024

REFERENCES

1. Morigny, P., Boucher, J., Arner, P., and Langin, D. (2021). Lipid and glucose metabolism in white adipocytes: pathways, dysfunction and therapeutics. Nat. Rev. Endocrinol. *17*, 276–295.
2. Klein, S., Gastaldelli, A., Yki-Järvinen, H., and Scherer, P.E. (2022). Why does obesity cause diabetes? Cell Metab. *34*, 11–20.
3. Scheja, L., and Heeren, J. (2019). The endocrine function of adipose tissues in health and cardiometabolic disease. Nat. Rev. Endocrinol. *15*, 507–524.
4. Divoux, A., Tordjman, J., Lacasa, D., Veyrie, N., Hugol, D., Aissat, A., Basdevant, A., Guerre-Millo, M., Poitou, C., Zucker, J.D., et al. (2010). Fibrosis in human adipose tissue: composition, distribution, and link with lipid metabolism and fat mass loss. Diabetes *59*, 2817–2825.
5. Mathis, D. (2013). Immunological goings-on in visceral adipose tissue. Cell Metab. *17*, 851–859.
6. Jimenez, M.T., Michieletto, M.F., and Henao-Mejia, J. (2021). A new perspective on mesenchymal-immune interactions in adipose tissue. Trends Immunol. *42*, 375–388.
7. Emont, M.P., Jacobs, C., Essene, A.L., Pant, D., Tenen, D., Colleluori, G., Di Vincenzo, A., Jørgensen, A.M., Dashti, H., Stefek, A., et al. (2022). A single-cell atlas of human and mouse white adipose tissue. Nature *603*, 926–933.
8. Feuerer, M., Herrero, L., Cipolletta, D., Naaz, A., Wong, J., Nayer, A., Lee, J., Goldfine, A.B., Benoist, C., Shoelson, S., and Mathis, D. (2009). Lean, but not obese, fat is enriched for a unique population of regulatory T cells that affect metabolic parameters. Nat. Med. *15*, 930–939.
9. Muñoz-Rojas, A.R., and Mathis, D. (2021). Tissue regulatory T cells: regulatory chameleons. Nat. Rev. Immunol. *21*, 597–611.
10. Cipolletta, D., Feuerer, M., Li, A., Kamei, N., Lee, J., Shoelson, S.E., Benoist, C., and Mathis, D. (2012). PPAR-γ is a major driver of the accumulation and phenotype of adipose tissue Treg cells. Nature *486*, 549–553.
11. Li, C., Wang, G., Sivasami, P., Ramirez, R.N., Zhang, Y., Benoist, C., and Mathis, D. (2021). Interferon-α-producing plasmacytoid dendritic cells drive the loss of adipose tissue regulatory T cells during obesity. Cell Metab. *33*, 1610–1623.e5.
12. Molofsky, A.B., Van Gool, F., Liang, H.E., Van Dyken, S.J., Nussbaum, J.C., Lee, J., Bluestone, J.A., and Locksley, R.M. (2015). Interleukin-33 and interferon-γ counter-regulate group 2 innate lymphoid cell activation during immune perturbation. Immunity *43*, 161–174.
13. Deng, T., Liu, J., Deng, Y., Minze, L., Xiao, X., Wright, V., Yu, R., Li, X.C., Blaszczak, A., Bergin, S., et al. (2017). Adipocyte adaptive immunity mediates diet-induced adipose inflammation and insulin resistance by decreasing adipose Treg cells. Nat. Commun. *8*, 15725.
14. Zhao, X.Y., Zhou, L., Chen, Z., Ji, Y., Peng, X., Qi, L., Li, S., and Lin, J.D. (2020). The obesity-induced adipokine sST2 exacerbates adipose T_{reg} and ILC2 depletion and promotes insulin resistance. Sci. Adv. *6*, eaay6191.
15. Spallanzani, R.G., Zemmour, D., Xiao, T., Jayewickreme, T., Li, C., Bryce, P.J., Benoist, C., and Mathis, D. (2019). Distinct immunocyte-promoting and adipocyte-generating stromal components coordinate adipose tissue immune and metabolic tenors. Sci. Immunol. *4*, eaaw3658.
16. Mahlakõiv, T., Flamar, A.L., Johnston, L.K., Moriyama, S., Putzel, G.G., Bryce, P.J., and Artis, D. (2019). Stromal cells maintain immune cell homeostasis in adipose tissue via production of interleukin-33. Sci. Immunol. *4*, eaax0416.
17. Burzyn, D., Kuswanto, W., Kolodin, D., Shadrach, J.L., Cerletti, M., Jang, Y., Sefik, E., Tan, T.G., Wagers, A.J., Benoist, C., and Mathis, D. (2013). A special population of regulatory T cells potentiates muscle repair. Cell *155*, 1282–1295.
18. Ali, N., Zirak, B., Rodriguez, R.S., Pauli, M.L., Truong, H.A., Lai, K., Ahn, R., Corbin, K., Lowe, M.M., Scharschmidt, T.C., et al. (2017). Regulatory T cells in skin facilitate epithelial stem cell differentiation. Cell *169*, 1119–1129.e11.
19. Biton, M., Haber, A.L., Rogel, N., Burgin, G., Beyaz, S., Schnell, A., Ashenberg, O., Su, C.W., Smillie, C., Shekhar, K., et al. (2018). T helper cell cytokines modulate intestinal stem cell renewal and differentiation. Cell *175*, 1307–1320.e22.
20. Hui, S.P., Sheng, D.Z., Sugimoto, K., Gonzalez-Rajal, A., Nakagawa, S., Hesselson, D., and Kikuchi, K. (2017). Zebrafish regulatory T cells mediate organ-specific regenerative programs. Dev. Cell *43*, 659–672.e5.
21. Liu, Z., Hu, X., Liang, Y., Yu, J., Li, H., Shokhirev, M.N., and Zheng, Y. (2022). Glucocorticoid signaling and regulatory T cells cooperate to maintain the hair-follicle stem-cell niche. Nat. Immunol. *23*, 1086–1097.
22. Li, C., Dispirito, J.R., Zemmour, D., Spallanzani, R.G., Kuswanto, W., Benoist, C., and Mathis, D. (2018). TCR transgenic mice reveal stepwise, multi-site acquisition of the distinctive fat-Treg phenotype. Cell *174*, 285–299.e12.
23. Subramanian, A., Tamayo, P., Mootha, V.K., Mukherjee, S., Ebert, B.L., Gillette, M.A., Paulovich, A., Pomeroy, S.L., Golub, T.R., Lander, E.S.,

and Mesirov, J.P. (2005). Gene set enrichment analysis: a knowledge-based approach for interpreting genome-wide expression profiles. Proc. Natl. Acad. Sci. USA *102*, 15545–15550.

24. Bäckdahl, J., Franzén, L., Massier, L., Li, Q., Jalkanen, J., Gao, H., Andersson, A., Bhalla, N., Thorell, A., Rydén, M., et al. (2021). Spatial mapping reveals human adipocyte subpopulations with distinct sensitivities to insulin. Cell Metab. *33*, 1869–1882.e6.
25. Kolodin, D., van Panhuys, N., Li, C., Magnuson, A.M., Cipolletta, D., Miller, C.M., Wagers, A., Germain, R.N., Benoist, C., and Mathis, D. (2015). Antigen- and cytokine-driven accumulation of regulatory T cells in visceral adipose tissue of lean mice. Cell Metab. *21*, 543–557.
26. Miyaoka, Y., Tanaka, M., Naiki, T., and Miyajima, A. (2006). Oncostatin M inhibits adipogenesis through the RAS/ERK and STAT5 signaling pathways. J. Biol. Chem. *281*, 37913–37920.
27. Elks, C.M., Zhao, P., Grant, R.W., Hang, H., Bailey, J.L., Burk, D.H., McNulty, M.A., Mynatt, R.L., and Stephens, J.M. (2016). Loss of oncostatin M signaling in adipocytes induces insulin resistance and adipose tissue inflammation *in Vivo*. J. Biol. Chem. *291*, 17066–17076.
28. Stephens, J.M., Bailey, J.L., Hang, H., Rittell, V., Dietrich, M.A., Mynatt, R.L., and Elks, C.M. (2018). Adipose tissue dysfunction occurs independently of obesity in adipocyte-specific oncostatin receptor knockout mice. Obesity (Silver Spring) *26*, 1439–1447.
29. Han, J., Wang, Y., Qiu, Y., Sun, D., Liu, Y., Li, Z., Zhou, B., Zhang, H., Xiao, Y., Wu, G., et al. (2022). Single-cell sequencing unveils key contributions of immune cell populations in cancer-associated adipose wasting. Cell Discov. *8*, 122.
30. Yang, J., Vamvini, M., Nigro, P., Ho, L.L., Galani, K., Alvarez, M., Tanigawa, Y., Renfro, A., Carbone, N.P., Laakso, M., et al. (2022). Single-cell dissection of the obesity-exercise axis in adipose-muscle tissues implies a critical role for mesenchymal stem cells. Cell Metab. *34*, 1578–1593.e6.
31. Delacher, M., Simon, M., Sanderink, L., Hotz-Wagenblatt, A., Wuttke, M., Schambeck, K., Schmidleithner, L., Bittner, S., Pant, A., Ritter, U., et al. (2021). Single-cell chromatin accessibility landscape identifies tissue repair program in human regulatory T cells. Immunity *54*, 702–720.e17.
32. Liu, F., He, J., Wang, H., Zhu, D., and Bi, Y. (2020). Adipose Morphology: a Critical Factor in Regulation of Human Metabolic Diseases and Adipose Tissue Dysfunction. Obes. Surg. *30*, 5086–5100.
33. DeMartinis, F.D., and Francendese, A. (1982). Very small fat cell populations: mammalian occurrence and effect of age. J. Lipid Res. *23*, 1107–1120.
34. Kirtland, J., Gurr, M.I., Saville, G., and Widdowson, E.M. (1975). Occurrence of "pockets" of very small cells in adipose tissue of the guinea pig. Nature *256*, 723–724.
35. Julien, P., Despres, J.P., and Angel, A. (1989). Scanning electron microscopy of very small fat cells and mature fat cells in human obesity. J. Lipid Res. *30*, 293–299.
36. Hansson, B., Wasserstrom, S., Morén, B., Periwal, V., Vikman, P., Cushman, S.W., Göransson, O., Storm, P., and Stenkula, K.G. (2018). Intact glucose uptake despite deteriorating signaling in adipocytes with high-fat feeding. J. Mol. Endocrinol. *60*, 199–211.
37. McLaughlin, T., Lamendola, C., Coghlan, N., Liu, T.C., Lerner, K., Sherman, A., and Cushman, S.W. (2014). Subcutaneous adipose cell size and distribution: relationship to insulin resistance and body fat. Obesity (Silver Spring) *22*, 673–680.
38. McLaughlin, T., Craig, C., Liu, L.F., Perelman, D., Allister, C., Spielman, D., and Cushman, S.W. (2016). Adipose Cell Size and Regional Fat Deposition as Predictors of Metabolic Response to Overfeeding in Insulin-Resistant and Insulin-Sensitive Humans. Diabetes *65*, 1245–1254.
39. Fang, L., Guo, F., Zhou, L., Stahl, R., and Grams, J. (2015). The cell size and distribution of adipocytes from subcutaneous and visceral fat is associated with type 2 diabetes mellitus in humans. Adipocyte *4*, 273–279.
40. McLaughlin, T., Sherman, A., Tsao, P., Gonzalez, O., Yee, G., Lamendola, C., Reaven, G.M., and Cushman, S.W. (2007). Enhanced proportion of small adipose cells in insulin-resistant vs insulin-sensitive obese individuals implicates impaired adipogenesis. Diabetologia *50*, 1707–1715.
41. Yang, J., Eliasson, B., Smith, U., Cushman, S.W., and Sherman, A.S. (2012). The size of large adipose cells is a predictor of insulin resistance in first-degree relatives of type 2 diabetic patients. Obesity (Silver Spring) *20*, 932–938.
42. Savage, D.B. (2009). Mouse models of inherited lipodystrophy. Dis. Model. Mech. *2*, 554–562.
43. Yu, S.Y., Luan, Y., Dong, R., Abazarikia, A., and Kim, S.Y. (2022). Adipose Tissue Wasting as a Determinant of Pancreatic Cancer-Related Cachexia. Cancers *14*, 4754.
44. Xiao, T., Langston, P.K., Muñoz-Rojas, A.R., Jayewickreme, T., Lazar, M.A., Benoist, C., and Mathis, D. (2022). T_{regs} in visceral adipose tissue up-regulate circadian-clock expression to promote fitness and enforce a diurnal rhythm of lipolysis. Sci. Immunol. *7*, eabl7641.
45. Sanchez-Infantes, D., and Stephens, J.M. (2020). Adipocyte oncostatin receptor regulates adipose tissue homeostasis and inflammation. Front. Immunol. *11*, 612013.
46. Albiero, M., Ciciliot, S., Rodella, A., Migliozzi, L., Amendolagine, F.I., Boscaro, C., Zuccolotto, G., Rosato, A., and Fadini, G.P. (2023). Loss of hematopoietic cell-derived Oncostatin M worsens diet-induced dysmetabolism in mice. Diabetes *72*, 483–495.
47. Komori, T., Tanaka, M., Senba, E., Miyajima, A., and Morikawa, Y. (2013). Lack of oncostatin M receptor β leads to adipose tissue inflammation and insulin resistance by switching macrophage phenotype. J. Biol. Chem. *288*, 21861–21875.
48. Komori, T., Tanaka, M., Senba, E., Miyajima, A., and Morikawa, Y. (2014). Deficiency of oncostatin M receptor β (OSMRβ) exacerbates high-fat diet-induced obesity and related metabolic disorders in mice. J. Biol. Chem. *289*, 13821–13837.
49. Piquer-Garcia, I., Campderros, L., Taxerås, S.D., Gavaldà-Navarro, A., Pardo, R., Vila, M., Pellitero, S., Martínez, E., Tarascó, J., Moreno, P., et al. (2020). A role for oncostatin M in the impairment of glucose homeostasis in obesity. J. Clin. Endocrinol. Metab. *105*, e337–e348.
50. Hanna, B.S., Wang, G., Galván-Peña, S., Mann, A.O., Ramirez, R.N., Muñoz-Rojas, A.R., Smith, K., Wan, M., Benoist, C., and Mathis, D. (2023). The gut microbiota promotes distal tissue regeneration via $ROR\gamma^{+}$ regulatory T cell emissaries. Immunity *56*, 829–846.e8.
51. Hui, S.P., Sugimoto, K., Sheng, D.Z., and Kikuchi, K. (2022). Regulatory T cells regulate blastemal proliferation during zebrafish caudal fin regeneration. Front. Immunol. *13*, 981000.
52. Liston, A., Nutsch, K.M., Farr, A.G., Lund, J.M., Rasmussen, J.P., Koni, P.A., and Rudensky, A.Y. (2008). Differentiation of regulatory $Foxp3^{+}$ T cells in the thymic cortex. Proc. Natl. Acad. Sci. USA *105*, 11903–11908.
53. Kim, J.M., Rasmussen, J.P., and Rudensky, A.Y. (2007). Regulatory T cells prevent catastrophic autoimmunity throughout the lifespan of mice. Nat. Immunol. *8*, 191–197.
54. Tomura, M., Yoshida, N., Tanaka, J., Karasawa, S., Miwa, Y., Miyawaki, A., and Kanagawa, O. (2008). Monitoring cellular movement in vivo with photoconvertible fluorescence protein "Kaede" transgenic mice. Proc. Natl. Acad. Sci. USA *105*, 10871–10876.
55. Wolf, F.A., Angerer, P., and Theis, F.J. (2018). SCANPY: large-scale single-cell gene expression data analysis. Genome Biol. *19*, 15.
56. Kuleshov, M.V., Jones, M.R., Rouillard, A.D., Fernandez, N.F., Duan, Q., Wang, Z., Koplev, S., Jenkins, S.L., Jagodnik, K.M., Lachmann, A., et al. (2016). Enrichr: a comprehensive gene set enrichment analysis web server 2016 update. Nucleic Acids Res. *44*, W90–W97.
57. Hao, Y., Hao, S., Andersen-Nissen, E., Mauck, W.M., III, Zheng, S., Butler, A., Lee, M.J., Wilk, A.J., Darby, C., Zager, M., et al. (2021). Integrated analysis of multimodal single-cell data. Cell *184*, 3573–3587.e29.

58. Love, M.I., Huber, W., and Anders, S. (2014). Moderated estimation of fold change and dispersion for RNA-seq data with DESeq2. Genome Biol. *15*, 550.

59. Schindelin, J., Arganda-Carreras, I., Frise, E., Kaynig, V., Longair, M., Pietzsch, T., Preibisch, S., Rueden, C., Saalfeld, S., Schmid, B., et al. (2012). Fiji: an open-source platform for biological-image analysis. Nat. Methods *9*, 676–682.

60. Akiyama, T.E., Sakai, S., Lambert, G., Nicol, C.J., Matsusue, K., Pimprale, S., Lee, Y.H., Ricote, M., Glass, C.K., Brewer, H.B., Jr., and Gonzalez, F.J. (2002). Conditional disruption of the peroxisome proliferator-activated receptor gamma gene in mice results in lowered expression of ABCA1, ABCG1, and apoE in macrophages and reduced cholesterol efflux. Mol. Cell. Biol. *22*, 2607–2619.

61. Felix, J.S., and Doherty, R.A. (1979). Amniotic fluid cell culture II. Evaluation of a red blood cell lysis procedure for culture of cells from blood-contaminated amniotic fluid. Clin. Genet. *15*, 215–220.

62. Picelli, S., Faridani, O.R., Björklund, A.K., Winberg, G., Sagasser, S., and Sandberg, R. (2014). Full-length RNA-seq from single cells using Smart-seq2. Nat. Protoc. *9*, 171–181.

63. Lopez, R., Regier, J., Cole, M.B., Jordan, M.I., and Yosef, N. (2018). Deep generative modeling for single-cell transcriptomics. Nat. Methods *15*, 1053–1058.

Please cite this article in press as: Wang et al., Adipose-tissue Treg cells restrain differentiation of stromal adipocyte precursors to promote insulin sensitivity and metabolic homeostasis, Immunity (2024), https://doi.org/10.1016/j.immuni.2024.04.002

STAR★METHODS

KEY RESOURCES TABLE

REAGENT or RESOURCE	SOURCE	IDENTIFIER
Antibodies		
Brilliant Violet 510™ anti-mouse CD45 (clone 30-F11)	Biolegend	Cat# 103138; RRID: AB_2563061
Pacific Blue™ anti-mouse TCR β chain (clone H57-597)	Biolegend	Cat# 109226; RRID: AB_1027655
Brilliant Violet 605™ anti-mouse CD4 (clone RM4-5)	Biolegend	Cat# 100548; RRID: AB_11125962
Brilliant Violet 711™ anti-mouse CD8a (clone 53-6.7)	Biolegend	Cat# 100759; RRID: AB_2563510
FITC anti-mouse Thy1.1 (clone OX-7)	Biolegend	Cat# 202504; RRID: AB_314014
PE/Cyanine7 anti-mouse ST2 (clone RMST2-2)	eBioscience	Cat# 25-9335-82; RRID: AB_2637464
Pacific Blue™ anti-mouse CD31 (clone 390)	Biolegend	Cat# 102422; RRID: AB_10613457
Brilliant Violet 605™ anti-mouse PDGFRα (clone APA5)	Biolegend	Cat# 135916; RRID: AB_2721548
PerCP/Cyanine5.5 anti-mouse Sca-1 (clone D7)	Biolegend	Cat# 108124; RRID: AB_893615
APC anti-mouse CD55 (clone RICO-3)	Biolegend	Cat# 131812; RRID: AB_2800632
PE/Cyanine7 anti-mouse Thy1.2 (clone 30-H12)	Biolegend	Cat# 105326; RRID: AB_2201290
Goat polyclonal anti-mouse IL-33	R&D	Cat# AF3626; RRID: AB_884269
Biotin anti-OSMR (clone 118125)	R&D	Cat# BAM662; RRID: AB_2156571
FITC anti-mouse Annexin V	BD Pharmingen	Cat# 556420; RRID: AB_2665412
Alexa Fluor® 700 anti-mouse Ki-67 (clone B56)	BD Pharmingen	Cat# 561277; RRID: AB_10611571
APC Streptavidin	BD Pharmingen	Cat# 554067; RRID: AB_10050396
Cy™3 AffiniPure™ Donkey Anti-Goat IgG (H+L)	Jackson Immunoresearch	Cat# 705-165-003; RRID: AB_2340411
Chemicals, peptides, and recombinant proteins		
Diphtheria Toxin	Sigma-Aldrich	Cat# D0564
2-Mercaptoethanol	Sigma-Aldrich	Cat# M7522
TCL RNA lysis buffer	Qiagen	Cat# 1031576
QIAzol Lysis Reagent	Qiagen	Cat# 79306
Recombinant Mouse Oncostatin M	Biolegend	Cat# 762802
Recombinant Mouse IL-33	Biolegend	Cat# 580502
Recombinant Human IL-2	Peprotech	Cat# 200-02
Bovine Insulin	Sigma-Aldrich	Cat# I0516
Dexamethasone	Sigma-Aldrich	Cat# D4902
Isobutylmethylxanthine	Sigma-Aldrich	Cat# I7018
Rosiglitazone	Cayman	Cat# 122320-73-4
16% Paraformaldehyde	Thermo Fisher	Cat# 50-980-487
Oil Red O	Sigma-Aldrich	Cat# O0625
Dynabeads™ Mouse T-Activator CD3/CD28	Thermo Fisher	Cat# 11452D
humulin R U-100 human insulin	Lilly	Cat# 0002-8215-01
Collagenase type II	Sigma-Aldrich	Cat# C6885
SuperScript™ III Reverse Transcriptase	Thermo Fisher	Cat# 18080044

(*Continued on next page*)

Continued

REAGENT or RESOURCE	SOURCE	IDENTIFIER
Critical commercial assays		
Foxp3 / Transcription Factor Staining Buffer Set	eBioscience	Cat# 00-5523-00
LIVE/DEAD Fixable Violet Dead Cell Stain Kit	Thermo Fisher	Cat# L34955
RNeasy Lipid Tissue Mini Kit	Qiagen	Cat# 74804
RNAClean XP beads	BeckmanCoulter	Cat# A63987
Nextera DNA Sample Prep Kit	Illumina	Cat# FC-121-1030
123count eBeads	Invitrogen	Cat# 01-1234-42
Mouse Oncostatin M Quantikine ELISA Kit	R&D	Cat# MSM00
PowerUp™ SYBR™ Green Master Mix for qPCR	Applied Biosystems	Cat# A25742
Deposited data		
Bulk RNA-seq of VmSC5s and Treg cells	This paper	GEO: GSE226889
Bulk RNA-seq of mouse VmSCs	Spallanzani et al.[15]	GEO: GSE126891
Bulk RNA-seq of mouse splenic and eVAT Treg cells	Li et al.[22]	GEO: GSE113393
Bulk RNA-seq of human Treg cells	Delacher et al.[31]	EGA: S00001004900
scRNA-seq of mouse VmSCs	Yang et al.[30]	GEO: GSE183288
scRNA-seq of human VmSCs	Han et al.[29]	NODE: OEP003500
Experimental models: Organisms/strains		
Mouse: B6.*Foxp3*^{Cre}	Jackson Laboratory	016959
Mouse: B6.Tg-*Pdgfra*^{Cre}	Jackson Laboratory	013148
Mouse: B6.Tg-*Adipoq*^{Cre}	Jackson Laboratory	028020
Mouse: B6.*Osmrb*$^{fl/fl}$	Jackson Laboratory	011081
Mouse: B6.*Foxp3*$^{Thy1.1}$	Liston et al.[52]	N/A
Mouse: B6.*Foxp3*^{Dtr}	Kim et al.[53]	N/A
Mouse: B6.*Kaede*	Tomura et al.[54]	N/A
Mouse: B6.*Osm*$^{fl/fl}$	Knockout Mouse Project	059829-UCD
Mouse: B6.*Pparg*$^{fl/fl}$	Cipolletta et al.[10]	N/A
Mouse: B6.*Pparg*^{Tdt}	Li et al.[22]	N/A
Oligonucleotides		
Primer: *Tbp* Forward: ACCCTTCACCAATGACTCCTATG	This paper	N/A
Primer: *Tbp* Reverse: TGACTGCAGCAAATCGCTTGG	This paper	N/A
Primer: *Osm* Forward: TCAAGCCACGAAGGGTCCTAA	This paper	N/A
Primer: *Osm* Reverse: GTCTTAAAGTCTCGGGTTTCACA	This paper	N/A
Primer: *Osmrb* Forward: CATCCCGAAGCGAAGTCTTGG	This paper	N/A
Primer: *Osmrb* Reverse: GGCTGGGACAGTCCATTCTAAA	This paper	N/A
Software and algorithms		
Scanpy v1.9.5	Wolf et al.[55]	https://scanpy.readthedocs.io/en/stable/
PRISM v10.2.0	GraphPad	https://www.graphpad.com/
Enrichr	Kuleshov et al.[56]	https://maayanlab.cloud/Enrichr/
R v4.2.2	The R Foundation	https://www.r-project.org
GenePattern	Broad Institute	http://software.broadinstitute.org/cancer/software/genepattern/

(*Continued on next page*)

Please cite this article in press as: Wang et al., Adipose-tissue Treg cells restrain differentiation of stromal adipocyte precursors to promote insulin sensitivity and metabolic homeostasis, Immunity (2024), https://doi.org/10.1016/j.immuni.2024.04.002

Continued

REAGENT or RESOURCE	SOURCE	IDENTIFIER
Seurat v4.0.3	Hao et al.[57]	https://satijalab.org/seurat/
DESeq2 v1.28.1	Love et al.[58]	https://bioconductor.org/packages/release/bioc/html/DESeq2.html
ImageJ v2.14.0	Schindelin et al.[59]	https://imagej.net/software/fiji/
Flowjo v10.1.0	BD Biosciences	https://www.flowjo.com/

RESOURCE AVAILABILITY

Lead contact

Further information and requests for resources and reagents should be directed to the lead contact, Diane Mathis (dm@hms.harvard.edu).

Materials availability

Mouse models generated in this study will be available upon request.

Data availability

Population-level RNA-seq data for mouse VmSCs, Treg cells and human Treg cells were extracted from GEO: GSE126891, GEO: GSE113393, and from the European Genome-phenome Archive (EGA) S00001004900, respectively. scRNA-seq data for mouse and human VmSCs were extracted from GEO: GSE183288 and the National Omics Data Encyclopedia (NODE: OEP003500), respectively. The accession number for the RNA-seq data generated in this paper is GEO: GSE226889.

EXPERIMENTAL MODEL AND PARTICIPANT DETAILS

Mouse models

Mice were maintained in our specific-pathogen-free (SPF) facilities at Harvard Medical School (HMS) on a low-fat diet (no. 5053, Lab Diet Picolab Mouse Diet 20). B6.*Foxp3-Cre* (016959), B6.Tg-*Pdgfra-Cre* (013148), B6.Tg-*Adipoq-Cre* (028020) mice were purchased from the Jackson Laboratory. B6.*Osmrb*^{fl} (011081) strain was retrieved out of cryopreservation and backcrossed to B6 for over 8 generations. B6.*Foxp3-Thy1.1*,[52] B6.*Foxp3-Dtr*,[53] B6.*Kaede*[54] and B6.*Osm*^{fl} (KOMP, Stock # 059829-UCD) mice were obtained from Drs. A. Rudensky, O. Kanagawa and R.A. Franklin. *Pparg*^{fl} and *Pparg-Tdt* mice were bred onto or generated on the B6 background in our laboratory as previously described.[22,60] Littermate controls were used for all experiments. Males were routinely used.

METHOD DETAILS

Animal treatment

For the Treg cell depletions, 12wk-old *Foxp3-Dtr*- or *Foxp3-Dtr*+ littermates were given 3 consecutive doses of DT (20ng/g body weight, D0564 Sigma) i.p., and were sacrificed at 14d after the last DT injection. For OSM gain-of-function, recombinant mouse OSM (40ng/g body weight, 762804 BioLegend) was i.p.-injected into DT-treated *Foxp3-Dtr*+ mice every other day for 7 doses.

Cell isolation and flow cytometry

eVAT was dissected, minced, and digested for 20min with 1.5 mg/ml collagenase type II (C6885 Sigma) in Dulbecco's Modified Eagle's Medium (DMEM) supplemented with 2% fetal calf serum (FCS) in a 37°C water bath with shaking. The digested material was filtered through a 100μm nylon cell strainer, digested with ACK (Ammonium-Chloride-Potassium) Lysing Buffer,[61] and then filtered through a 40 μm nylon cell strainer. The stromal vascular fraction (SVF) was collected after centrifugation at 650g for 5 min. For T lymphocyte analysis, cells were stained with anti-CD45 (30-F11), -TCRβ (H57-597), -CD4 (RM4-5), -CD8a (53-6.7) and -Thy1.1 (OX-7) mAbs (all from BioLegend); anti-ST2 (RMST2-2) (eBioscience); and LIVE/DEAD Fixable Violet Dead Cell Stain Kit (Invitrogen) or DAPI. For VmSC analysis, cells were stained with anti-CD45 (30-F11), -CD31 (390), -PDGFRα (APA5), -Sca-1 (D7), -CD55 (RICO-3) and -Thy1.2 (30-H12) mAbs (all from BioLegend); anti-Annexin V (Cat#: 556420, BD Pharmingen) and LIVE/DEAD Fixable Violet Dead Cell Stain Kit (Invitrogen) or DAPI. Cells were fixed, permeabilized, and intracellularly stained for IL-33 (Cat#: AFS626, R&D), OSMR (Cat#: BAM662, R&D) or Ki67 (B56, BD Pharmingen) at 4°C overnight followed by donkey anti-goat IgG secondary antibody (Jackson Immunoresearch) or APC-streptavidin (Cat#: 554067, BD Pharmingen) at room temperature for 1 hour according to the manufacturer's instructions (eBioscience). Cells were acquired using LSRII or FACSymphony A5 flow cytometers (BD Biosciences) and were sorted using a FACSAria (BD) cell sorter. Data were analyzed using FlowJo software.

Cell culture and adipogenesis assay

Sorted VmSCs from 12wk-old *Pparg-Tdt* mice were cultured in growth medium (DMEM/F12 supplemented with 10% fetal bovine serum (FBS) and 1% penicillin/streptomycin) for 2 days and switched to pro-adipogenic medium I (growth medium with 5μg/mL bovine insulin, 1μM dexamethasone, 1μM Isobutylmethylxanthine from Sigma and 1μM rosiglitazone from Cayman) for 2 days followed by pro-adipogenic medium II (growth medium with 5μg/mL bovine insulin and 1μM rosiglitazone) for 2 days. Cells were fixed with 4% paraformaldehyde for 30 min at room temperature, 60% isopropanol for 5 min and stained with 1.2mg/mL Oil-Red-O (Sigma) in 60% isopropanol for 5 min followed by DAPI for 1 hour. Cells were imaged using a Nikon Ti inverted microscope and analyzed using Fiji software.

For the preparation of the conditioned medium, eVAT-Treg cells were sorted from 12wk-old *Foxp3-Thy1.1* mice, cultured in RPMI1640 supplemented with 10% FBS, 50μM β-mercaptoethanol, 1% penicillin/streptomycin, 2000U/mL human recombinant IL-2 (Cat# 200-02, Peprotech), 20ng/mL mouse recombinant IL-33 (Cat# 580506, BioLegend), and were stimulated with anti-CD3/CD28 dynabeads (Cat# 11452D, ThermoFisher) for 2 days at 37°C in a 5% CO2 atmosphere. Supernatant from the cultured eVAT-Treg cells was collected as eVAT-Treg CM.

Histology

The eVAT depot was fixed in 10% formalin and processed by the Rodent Histopathology Core at HMS. Four sections, 100 μm apart, from each sample were stained with H&E. Sections were imaged using a Nikon Ti inverted microscope and analyzed using Fiji software.

ITTs and GTTs

12wk-old mice were fasted for 4 hours before being injected i.p. with insulin (0.75 unit/kg body weight, Humulin R, Lilly) or glucose (1g/kg body weight). Blood-glucose levels were measured 0, 20, 40, 60, 90, and 120 minutes after injection. For the ITTs, data were normalized to the blood-glucose levels at 0min. and the area over the curve (AOC) was calculated using GraphPad Prism. For the GTTs, the area under the curve (AUC) was calculated using GraphPad Prism.

Quantification of gene expression by RT-qPCR

RNA was extracted from the sorted cells and purified using the RNeasy Lipid Tissue Mini Kit (QIAGEN) according to the manufacturer's instructions. cDNA was synthesized using SuperScript III Reverse Transcriptase (Thermo Fischer Scientific). Real-time quantitative PCR (RT-qPCR) was performed using SYBR Green-based assays (Applied Biosystems). Transcript values were normalized to those for the mouse *Tbp* gene (FWD: ACCCTTCACCAATGACTCCTATG; REV: TGACTGCAGCAAATCGCTTGG). Primers that detect *Osm* and *Osmrb* were employed for PCR titration of transcript levels (*Osm* FWD: TCAAGCCACGAAGGGTCCTAA; REV: GTCTTA AAGTCTCGGGTTTCACA; *Osmrb* FWD: CATCCCGAAGCGAAGTCTTGG; REV: GGCTGGGACAGTCCATTCTAAA).

Bulk RNA-seq library preparation and data analysis

For VmSCs, 1,000 cells were double-sorted into 5ul Buffer TCL (QIAGEN) with 1% 2-Mercaptoethanol (Sigma). For the floating adipocytes, RNA was extracted and purified using RNeasy Lipid Tissue Mini Kit (QIAGEN) according to the manufacturer's instructions, and 2ng RNAs were added to 5ul Buffer TCL (QIAGEN) with 1% 2-Mercaptoethanol (Sigma). Library construction and sequencing as well as data processing were performed according to standard Immunological Genome Project protocols (https://www.immgen.org/img/Protocols/ImmGenULI_RNAseq_methods.pdf). Smart-seq2 libraries were prepared and sequenced as previously described.[62] Briefly, RNA was captured and purified using RNAClean XP beads (Beckman Coulter), and polyadenylated (poly-A) mRNA was selected using an anchored oligo(dT) primer (5′-AAGCAGTGGTATCAACGCAGAGTACT30VN-3′). Poly-A mRNA was converted to cDNA by the reverse-transcription reaction followed by limited PCR amplification of first-strand cDNA. The Nextera XT DNA Library Preparation Kit (Illumina) was used for Tn5 transposon-based fragmentation followed by PCR amplification for an additional 12 cycles using barcoded primers such that each sample carried a specific combination of Illumina P5 and P7 barcodes. Paired-end sequencing was performed on an Illumina NextSeq500 (two full NextSeq runs per plate for an average of 10M raw reads per sample) using two 38-bp reads with no further trimming. Reads were aligned to the mouse genome (GENCODE GRCm38/mm10 primary assembly and gene annotations vM16) using STAR 2.7.3a. Transcripts annotated as ribosomal RNA were removed, and gene-level quantification was calculated using the Subread 2.0 command featureCounts. The DESeq2 package from Bioconductor was used to normalize raw read counts according to the median of ratios method (samples with <1 million uniquely mapped reads or with fewer than 8000 genes with over 10 reads were excluded from normalization). Normalized data were converted to GCT and CLS files, which were used in downstream analyses. Additional quality control after normalization included removal of biological replicates with a poor Pearson's correlation (<0.9) and/or poor congregation by principal component analysis of the top 1000 variable genes. Normalized reads were further filtered by minimal expression over 10. Data were analyzed by Multiplot Studio in the GenePattern software package and EnrichR.[56] The adipogenesis up-signature came from Gene Set Enrichment Analysis (GSEA).[23]

scRNA-seq analysis

Two previously published single-cell datasets containing VAT samples from mice[30] and humans[29] were reanalyzed. The processed RDS files or count matrices were downloaded from GEO for the mouse (GEO: GSE183288) and from the National Omics Data Encyclopedia (NODE: OEP003500) for the human samples. Single-cell data were reanalyzed using the Seurat or Scanpy packages using

Please cite this article in press as: Wang et al., Adipose-tissue Treg cells restrain differentiation of stromal adipocyte precursors to promote insulin sensitivity and metabolic homeostasis, Immunity (2024), https://doi.org/10.1016/j.immuni.2024.04.002

standard pipelines.[55,57] Low-quality cells with percentages of mitochondrial transcripts over 15 were excluded from the human dataset, and only samples from sedentary mice fed a low-fat diet and non-cachexic humans were selected for further analysis. VmSCs were identified as *Pdgfra*$^{+}$*Msln*$^{-}$ and *PDGFRA*$^{+}$*MSLN*$^{-}$ for the mouse and human datasets, respectively. The human samples were aligned using scvi to perform dimensionality reduction.[63] The genes most highly correlated with *Osmrb* in mouse VmSCs were found by calculating the Spearman correlation between all genes and *Osmrb* across mouse VmSCs. The 50 genes with the highest rho values were selected, converted to their human homologs, and then plotted as a signature using the score_genes function in Scanpy.

QUANTIFICATION AND STATISTICAL ANALYSIS

Data are presented as mean ± SD. Significance was assessed by Student's t-test for two-groups comparisons, ANOVA for multiple-group comparisons or the Kolmogorov-Smirnov test for adipocyte size distribution using GraphPad Prism 7.0. To assess the significant enrichment of gene signatures in RNA-seq datasets, we used a Chi-square test. P = *, < 0.05; **, < 0.01; ***, < 0.001; ****, < 0.0001.